University of Padova
Academic year 2015-2016 (794th)
Department of Industrial Engineering (DII)
Master's thesis in Aerospace Engineering

FELDs: mechanical design and development of a tethered soft docking setup for microgravity testing

Author: Alessandro Cavinato
Supervisor: Alessandro Francesconi

To my family, who supported me during this challenging experience

Abstract

Rendezvous and docking maneuvers have been performed in orbit for more than 40 years; the physical connection between two spacecraft is necessary for several important activities such as fuel, crew and material transfer. Docking is the last phase of a rendezvous, in which the two spacecraft physically connect through the use of a suitable mechanism.

Flexible Electromagnetic Leash Docking system (FELDs) is a technology demonstrator that tested the performance of an innovative tethered soft docking mechanism. The experiment has been selected by the European Space Agency (ESA) education office, Esa Education, for the Drop Your Thesis! (DYT) campaign in 2014. This Esa Education program provides every year the opportunity, for just only a university student team in whole Europe, to test an experiment in microgravity condition exploiting the Center of Applied Space Technology and Microgravity (ZARM) Drop Tower in Bremen.

This thesis presents the design and development of of the proposed docking technology; two major subsystems form the docking simulator, a damped target subsystem, provided with load measurement sensors, and a launch unit, provided with a shoot mechanism to eject the probe towards the target. Relevant focus is given to the mechanical response of the docking simulator due to the impact of the probe on the target subsystem, reporting a comparison between the theoretical results and the data collected in microgravity.

Contents

Chapter 1

Introduction

Flexible Electromagnetic Leash Docking system (FELDs) is a technology demonstrator that tested the performances of an innovative tethered soft docking system. The docking is performed by launching a ferromagnetic probe towards the target, which attracts it with a static magnetic field. As the connection between the probe and the launching spacecraft is flexible, the system is self-adjusting, with no need for precise positioning and attitude control. The experiment aimed to understand the low gravity behavior of the proposed technology by studying the dynamic response of the capture system and its effects on the target spacecraft. The main experiment objective was to build and test an electromagnetic docking system that guarantees a mechanical connection through the use of a flexible wire and to study the magnetic capture effect on the probe. The experiment objective was accomplished in semi-realistic orbit conditions: the Center of Applied Space Technology and Microgravity (ZARM) Drop Tower (Fig. 1.1) is a facility that let to reproduce the Low Earth Orbit (LEO) orbit microgravity environment.

Fig. 1.1: ZARM Drop Tower

The gravity levels that are obtained in ZARM Drop tower experiments are as low as 10^{-6}g and last for about 5 to 10 seconds. This is closed to level that attained for experiments on the International Space Station (ISS). The tower is 146 meters high and the experiment is mounted into a capsule and released from 120 meters height in a near vacuum providing approximately 4.74 seconds microgravity. At the end of the experiment the capsule is decelerated into a deceleration chamber rapidly to 50g.

According to an exhaustive bibliographic research, tethered docking is still a largely unexplored field, although the interest in this technology is growing in the international space community. During the campaign five test were performed, and many data were collected allowing the technology validation and laying the basis for future development and implementation of systems based on the original idea.

1.1 Actual docking technologies

Several important activities such as crew, fuel and material transfer required a physical connection between two spacecrafts. The joining between two space vehicles is obtained with a docking system. Docking represents the last phase of a rendezvous maneuver between two approaching objects, in which the actual physical link is achieved. Docking mechanisms consist in very sophisticated technologies, enabling crew members to move between two vehicles and to transfer electric power and propellant between linked ships. An example of simple docking configuration is represented in the following picture. (Fig. 1.2).

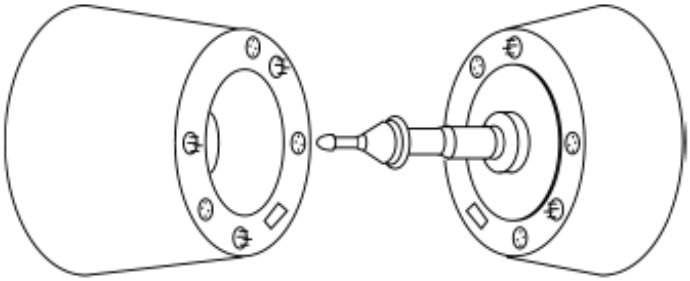

Fig. 1.2: Classic Docking system

One of the most important example is represented by the Soyuz docking mechanism [1]. The Soyuz docking system is composed by an active docking assembly and a passive docking assembly. This type of docking system is called the probe and cone, or "Classic", type and is shown in Fig. 1.3 and is integrated on the transfer hatch of the Soyuz vehicle. Firstly the system corrects initial vehicle misalignments and then dampens the impact energy: during the docking operation the probe can be extended and retracted by the docking mechanism drive. The head of the front probe is provided with four latches, which are extended and retracted by the latch drive. The so called "touchdown" consists in the moment when the probe head firstly touches the cone. After the probe head latches are locked in the socket, the docking mechanism attracts both vehicles together and mutually aligns them.

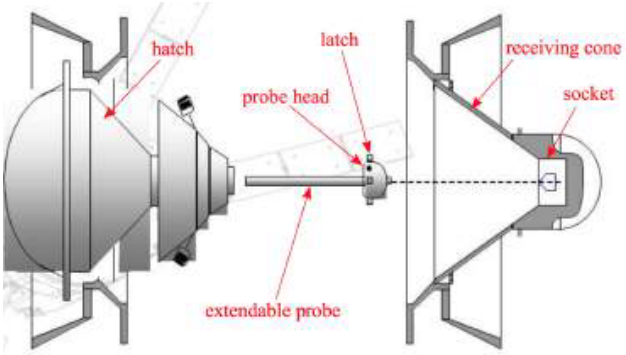

Fig. 1.3: Soyuz Docking system

The above described rigid mechanical approach guarantees structural rigidity and a strong connection between the involved spacecrafts but has considerable disadvantages. Performing an approach between two stiff objects is really challenging because of the mechanical complexity and strict pointing/control requirements needed. These severe restrictions constrain the operation flexibility of the entire system, enlarging docking system components' masses and are not scalable for small satellites.
An example of docking mechanism designed for Micro and Nanosatellites is represented by the Synchronized Position Hold, Engage, Reorient, Experimental Satellites (SPHERES) docking system [2], depicted in Fig. 1.4, that features an androgynous pin-hole architecture that is common to each module and allows not only a rigid mechanical connection, but also fluids, power and data transfer.

Fig. 1.4: SPHERES Docking system

Its main drawbacks are represented by the exploitation of moving mechanical parts and the need for the modules to be oriented in a specific way on the roll axis in order to accomplish docking, as the interface is androgynous but not symmetric.
In addition to SPHERES, only few other connection systems for small-scale spacecraft have been developed to date, mostly based on the probe-receptacle configuration. For instance, the Autonomous Microsatellite Docking System (AMDS) (Fig. 1.5) [3] of Michigan Aerospace exploits an extendable probe, which is captured by the drogue and then retracts, causing the two vehicles to mate before a series of mechanical latches secure the connection.

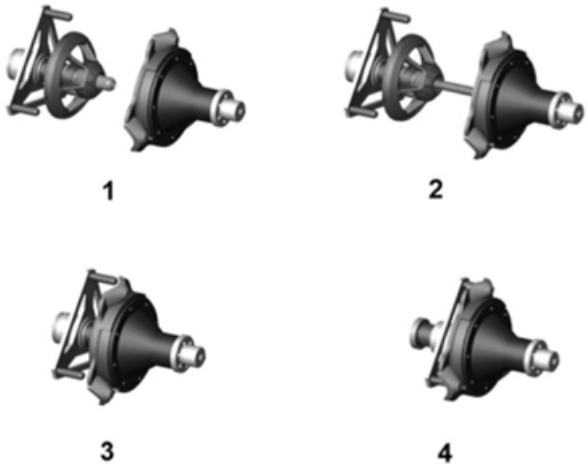

Fig. 1.5: AMDS Docking system

Another example is given by the Autonomous Rendezvous Control And Docking Experiment (ARCADE) docking system (Fig. 1.6) [4] that is based on a concept similar to the Soyuz docking system but for smaller vehicles. The University Center of Space Studies and Activities (CISAS) "G.Colombo" research group (University of Padova) developed ARCADE in the framework of the Rocket/Baloon Experiment for University Students (REXUS/BEXUS) program, an Swedish National Space Board (SNSB)/German Aerospace Center (DLR) campaign (in collaboration with ESA) that allows students from universities and higher education colleges across Europe to carry out scientific and technological experiments on research rockets and balloons.

The ARCADE docking mechanism is composed of a probe with a steel tip, which is captured by an electromagnet placed at the end of the drogue; a linear actuator pulling action performs the docking maneuver until three latches lock the probe in position.

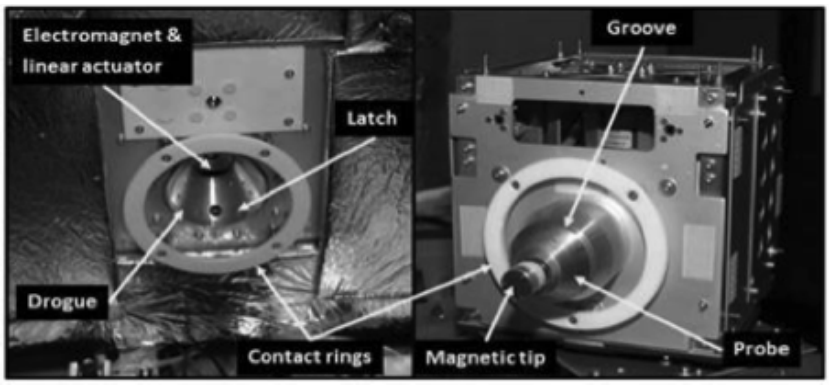

Fig. 1.6: ARCADE Experiment

The CISAS "G. Colombo" group also developed another small-scale docking system (Fig. 1.7) that uses a semi-androgynous shape-shifting mechanism [6]; one of the two interfaces shifts into a "drogue" configuration, letting the other port penetrate and close around it to create a solid joint.

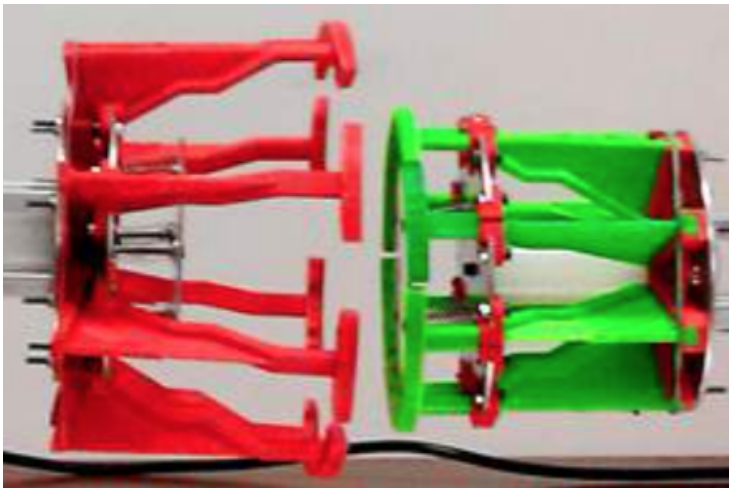

Fig. 1.7: CISAS Semi androgynous docking system

Magnetic docking mechanisms for small satellites have never been tested before. A large-scale androgynous magnetic soft docking system was studied and patented [5] by National Aeronautics and Space Administration (NASA) (Fig. 1.8), but its structure is not easily adaptable to smaller sizes. Its original function was the docking of visiting spacecraft and the berthing of the Crew Return Vehicle (CRV) at the International Space Station. The system is composed of an active subsystem on one spacecraft and a passive subsystem on the other spacecraft. In preparation for docking, one spacecraft would move to a position near the other spacecraft, with the docking ports of the two spacecraft in approximate alignment. Then, while one spacecraft maintains an approximately constant position relative to the other spacecraft, the actuators of the active subsystem would extend the ring, gently pushing the guide petals and magnetic striker plates: in effect, the active subsystem would reach out, attract, and grab the passive subsystem.

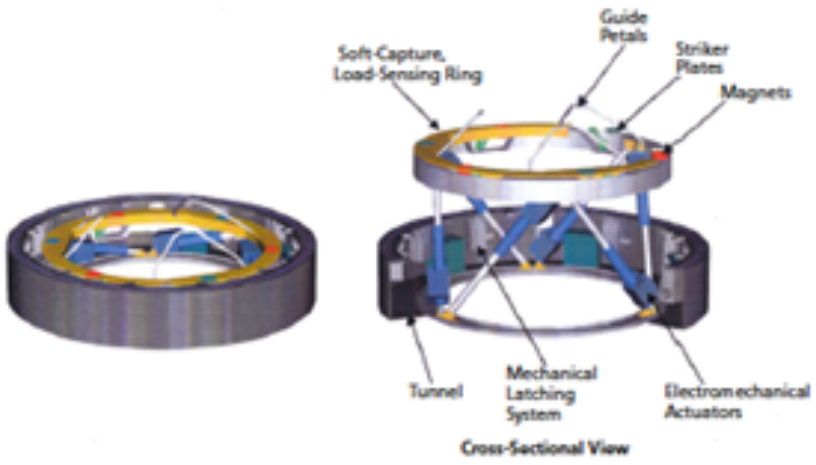

Fig. 1.8: ISS NASA Docking system (Courtesy of NASA)

1.2 FELDs Experiment

In this framework, a new approach to overcome some of the drawbacks listed above (accurate attitude and aligning control, close distances for approach, high fuel consumption) was conceived by the FELDs team building an electromagnetic docking system that guarantees the mechanical connection by using a flexible wire. The docking is performed by launching a ferromagnetic probe (linked with the wire) towards the target, which attracts it with a static magnetic field. As the connection between the probe and the launching spacecraft is flexible, the system is self-adjusting, with no need for precise positioning and attitude control. Another advantage of this kind of system over traditional docking mechanisms is the low impact force: as the probe mass is almost negligible when compared to the target satellite mass (1-5 %), the soft docking attempt does not disturb the target spacecraft trajectory and its attitude. After the successful soft docking, the target can be reeled in by retracting the wire and a traditional hard dock can be performed, controlling the tether tension to dampen the residual relative motion of the two spacecraft. This would allow unmanned docking even with a non-cooperative target spacecraft, a maneuver considered extremely challenging. The FELDs experiment has two main objectives: the first is to test and validate the performance of the FELDs docking system, assessing the reliability of the electromagnetic effect of the target subsystem on the probe (magnetic guide and consequent capture), while the second is to study the dynamics of the target system and the chaser during and after the impact. In order to achieve these objectives, the dynamics of the encounter events were monitored during the experiment (e.g., forces and torques between the probe and the target) and the kinematics of the probe/tether system and the approach system were studied using a set of dedicated sensors and camcorders in relation to the operating conditions. The results are extremely useful to understand the in-orbit behavior of a free-floating spacecraft touched by a tethered probe in the framework of a docking maneuver and to evaluate the system concept feasibility and the possible limitations of the proposed technology.

1.3 Experiment layout

The image below shows the drawing of the entire system integrated on the capsule used during the Drop tests (Fig. 1.9).

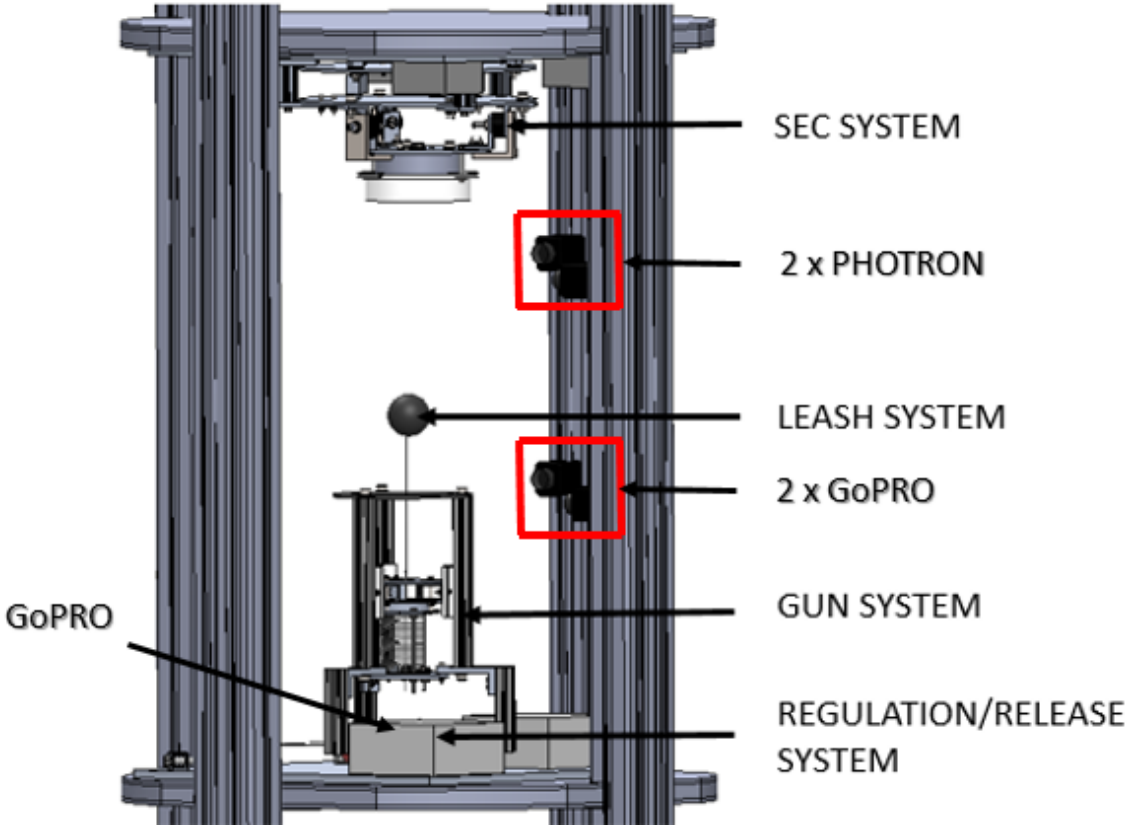

Fig. 1.9: FELDs experiment

The four captions in the picture indicate the four subsystems that together form FELDs. The two major subsystems are the Sensor Electromagnet and Cap (SEC) system and the GUN system. The SEC system, mounted on the upper capsule platform, represents the target interface of the electromagnetic docking setup, and has the role to guide and capture the ferromagnetic chaser through a static magnetic field generated by an off-the-shelf electromagnet. This subsystem is provided with load sensors to analyze the target response after a successful connection, thus allowing to understand the effects of vibrations on the target spacecraft. The GUN,

mounted in the lower platform, represents the launch unit, and has the role to provide the right spring compression for the Leash system (the set of a Kevlar^{TM} wire, also called tether, and the ferromagnetic sphere, which represents the chaser). The Leash system is kept tense before the shot by the Regulation system which consists in a mechanism designed to vary the spring's initial compression, thus allowing to perform launches with different probe's velocities. The Release system, consisting in a costantan wire inlaid in an electrical connector, allows an instantaneous spring decompression and consequent wire release.

1.3.1 Capsule schematics

The following rendering shows how the experiment was mounted in the ZARM capsule (Fig. 1.10).

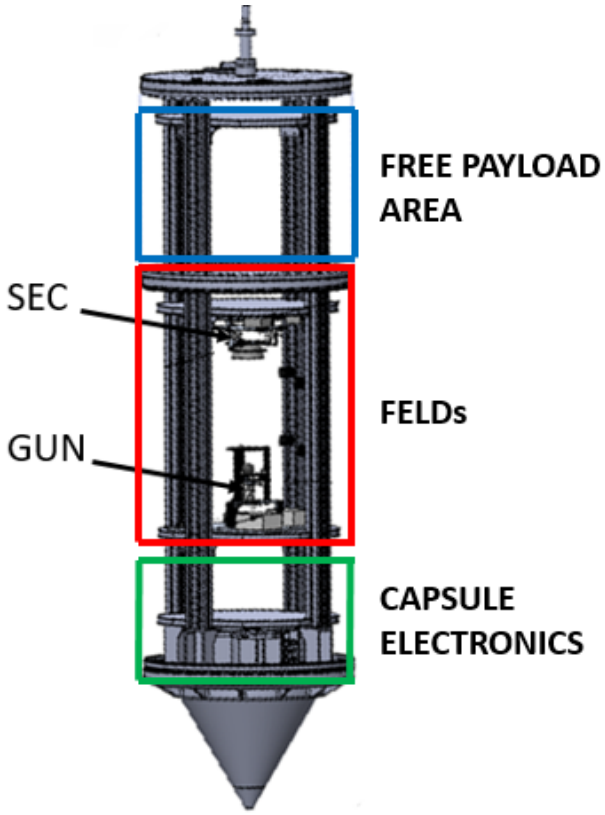

Fig. 1.10: Capsule schematics

The SEC has been positioned on the upper platform of the ZARM Drop Capsule, while the GUN has been positioned in the lower part of the payload. Both the major experiment subsystems has been placed inside the capsule in order to have their center of mass located along the z-axis of the capsule. In order to evaluate the dynamics of the tethered system four high-speed cameras were placed along the trajectory of the probe: two Photron cameras provided by ZARM were placed at the same height and at a right angle to each other, while the other two GoPro cameras were placed 20 cm below the first pair in order to capture the whole trajectory (Fig. 1.11).

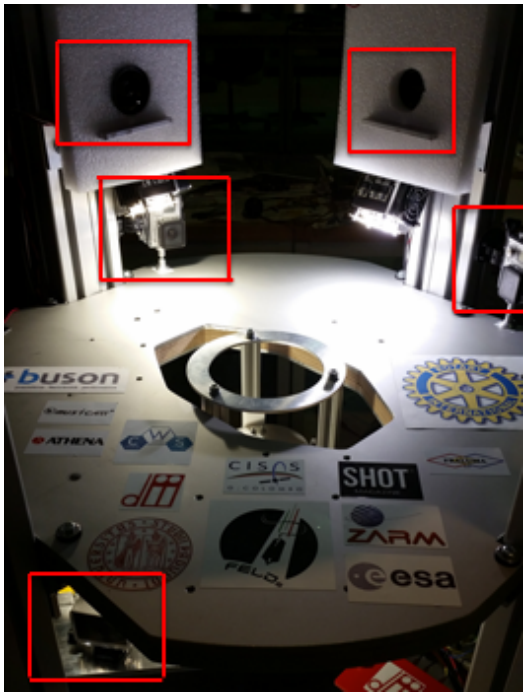

Fig. 1.11: Positions of cameras inside the capsule

Each image has been considered separately and the Hough transform was applied in order to find the spherical probe, which shows as a circle in recorded images from all angles. The position of the probe has been interpolated with Euclidean geometry.
During the week before the Drop Campaign in Bremen another GoPro Hero 3+ Silver has been installed to record the tether release. Summarizing, FELDs was provided with a total of 5 high frame rate cameras, for two

main objectives:

- a qualitative evaluation of the performance of the release system
- recording the probe's ascent phase towards the SEC and extracting its trajectory in threedimensional space

To record the tether release a GoPro Hero 3+ Silver has been used at 100 fps. The other four cameras were used to measure the trajectory of the probe and were calibrated by identifying the probe in several known positions and finding a linear conversion matrix by minimum square interpolation. The cameras were placed in two pairs at difference heights. The upper pair of cameras were Photron Fastcams provided by ZARM with a frame rate of 1000 fps and a resolution of 512 x 512 pixels. The lower pair were GoPro Hero 3+ Black cameras, with a frame rate of 100 fps and a resolution of 1280 x 960 pixels.

1.4 Thesis outline

The rest of the Thesis is organized as follows: chapter 2 and chapter 3 presents respectively a detailed description of the SEC and GUN systems, retracing the steps of the mechanical design process of the two major subsystems of the docking simulator, including the structural verification of the various subsystem due to the significant deceleration (50g) acting on the capsule during the landing phase. Relevant focus will be given on the design process of the load measurement system of the SEC. Chapter 4 presents the mechanical response of the target subsystem due to the impact with the chaser, reporting the data collected during the five tests performed, while chapter 5 contains the conclusions and some possible future design improvements of the proposed technology.

Chapter 2

SEC system

The target unit consists in a multi-layered structure, designed in order to implement the target interface of a real spacecraft's docking system (Fig. 2.1).

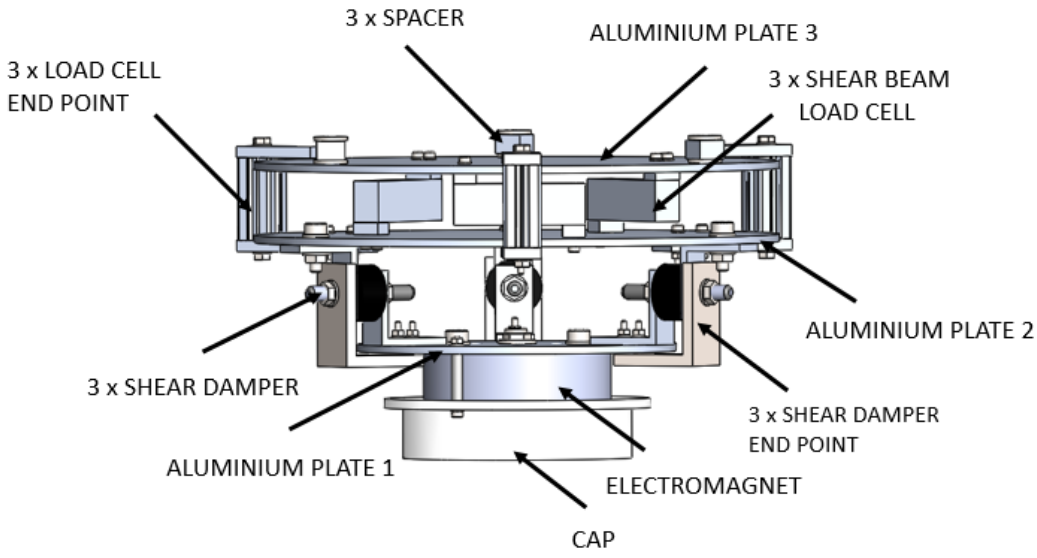

Fig. 2.1: SEC system

In the first phases of the design process, two different layout were considered for this subsystem:

- a rigid version, to measure the forces acting on the electromagnet

- a damped version, to study the impact effects of the probe on a realistic system

Giving the priority to the technological trial, the first version mentioned has been discarded because the idea of a rigid SEC would have brought little meaningful data. The decision of inserting damping in the structure has been essential to achieve a closer representation of a real target system since the layered structure, exploiting the dampers action, allows the sensors of the load cells to obtain important data about impact force and system mechanical response, thus allowing the characterization of the soft docking. The damped feature of the receiving interface also avoid the probe from bouncing on the electromagnet, hitting other subsystems and damaging them.

2.1 Mechanical description

Starting from the bottom, the electromagnet is covered by a plastic Cap (Fig. 2.2) which has been designed to facilitate the probe capture in case of misaimed shot.

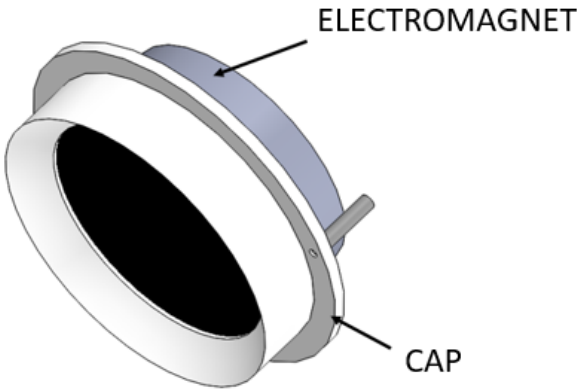

Fig. 2.2: Cap mounted on the electromagnet, above view

The Cap inner surface has a parabolic shape with the focus coincident with the center of the electromagnet: when a misaligned launch occurs, this component has the role to slow down the probe and send it towards the

center of the electromagnet. The Cap has been drawn and then printed with a 3D printer. The electromagnet, (in both configurations within and without the Cap), is mounted on a 170 mm diameter, 4 mm thick, aluminium plate (1) with three M6 screws arranged at 120 degrees and a central M8 screw (Fig. 2.3). When used, the Cap is also fixed on the aluminium plate 1 with two M3 screws arranged at 180 degrees.

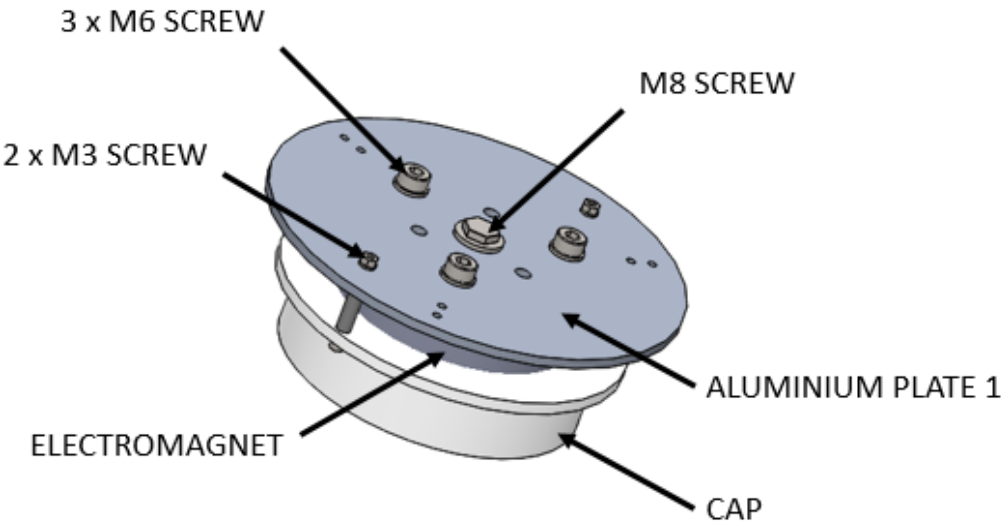

Fig. 2.3: Electromagnet and Cap mounted on aluminum plate 1

The structure's damping properties are obtained exploiting the action of three shear dampers, placed between aluminium plate 1 and aluminium plate 2 (Fig. 2.4).

To house the dampers three L (1) profiles are mounted in the upper side of plate number 1 with two M3 screws aligned each. The three dampers are mounted on the external side with three more L (2) profiles on a 280 mm diameter, 4 mm thick, aluminium plate (2) with three M6 screws each. On the external side of the L profiles connected to plate 2, three additional steel L profiles are mounted and act as a safety block, leaving 0.25 mm play in order to allow the right dampers deflection, while preserving the structure's integrity during the capsule's impact with the ground. To characterize the docking and determine the target system's response to the impact with the probe, three shear beam load cells are placed between plate 2 and plate three

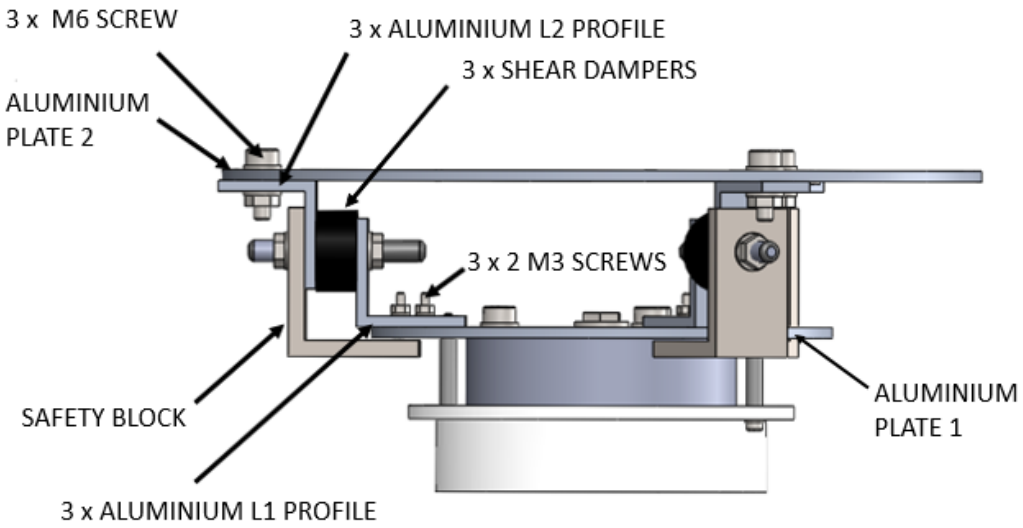

Fig. 2.4: Damper housing between plate 1 and plate 2

(Fig. 2.5). The last aluminium plate (3) has the same diameter and thickness of plate 2, and acts ad a fixed reference frame.

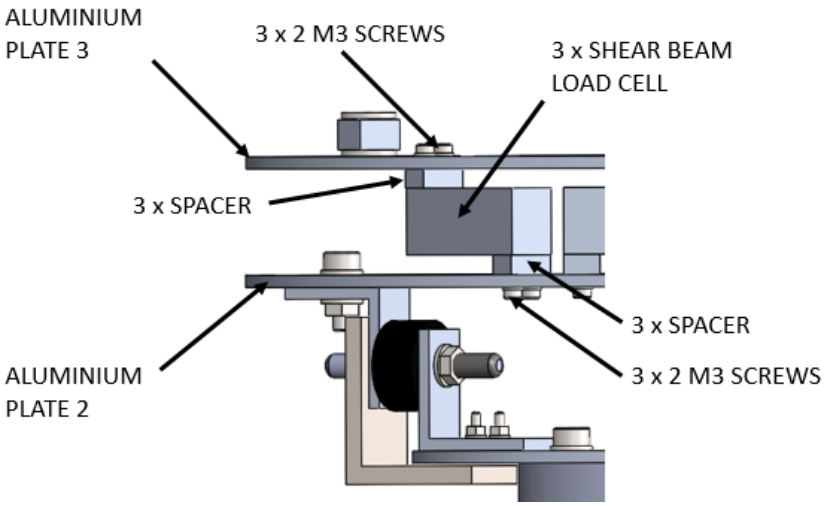

Fig. 2.5: Shear beam load cells' mounting between plate 2 and plate 3

The three load cells are fixed to both the plates by two M3 screws placed at 7 mm, and between each load cell and the plates small spacers are added in order to protect the piezoresistive element of the sensors. The load cells' maximum warping is 0.4 mm: for this reason, to prevent the cells form being

damaged at the impact of the capsule with the ground during the landing phase, a protection system has been designed (Fig. 2.6). The protection system is composed by a 20 x 20 mm Bosch^{TM} profile connected to two aluminium bars by two M5 screws. The lower bar is connected to plate 2 by two aligned M3 screws, while the upper bar has a 0.4 mm travel with plate 3, thus allowing the complete deflection of the load cells, while avoiding any damage.

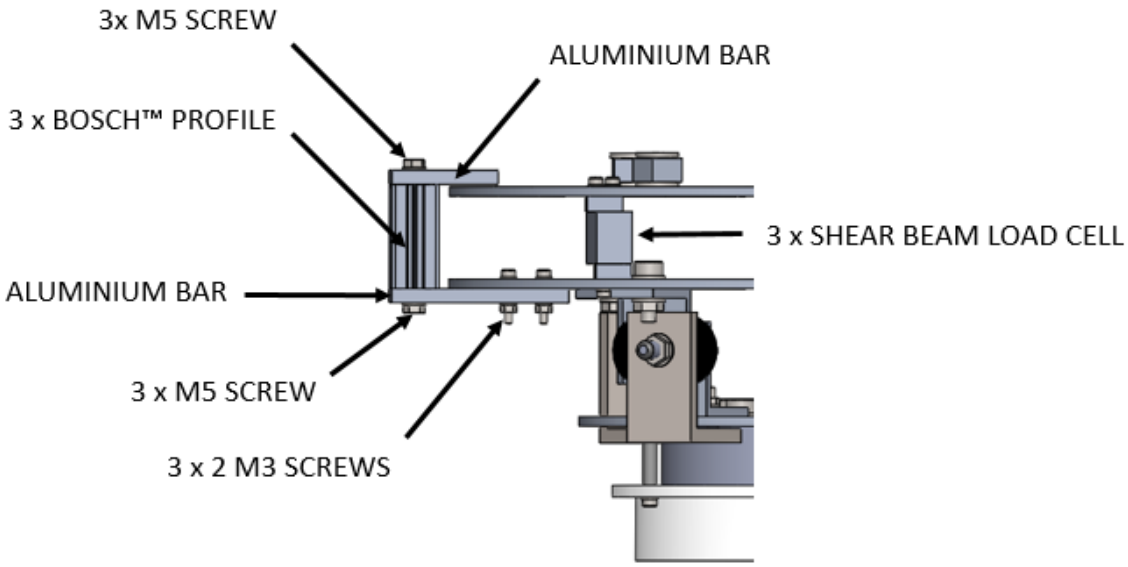

Fig. 2.6: Shear beam load cells' protection system

The entire system has been integrated in the upper platform of the ZARM capsule with three M6 screws which connect the platform and plate 3 (Fig. 2.7 - Fig. 2.8). Between the plate and the platform three adjustable length spacers were inserted, in order to vary the distance between the SEC and the GUN during the test campaign.
As the matter of fact the first four Drops has been preformed with a distance of 340 mm between the SEC and the GUN while the last Drop has been executed with a probe flight distance of 410 mm.

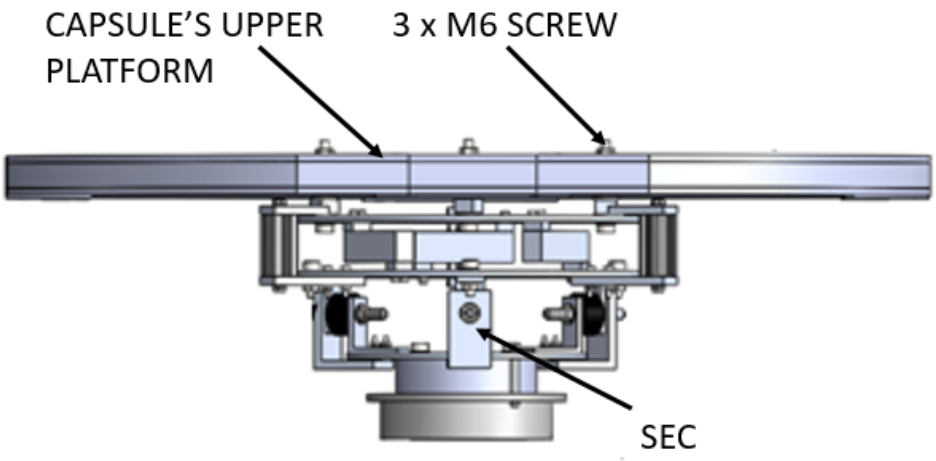

Fig. 2.7: SEC mounted in the ZARM capsule's upper platform, rendering

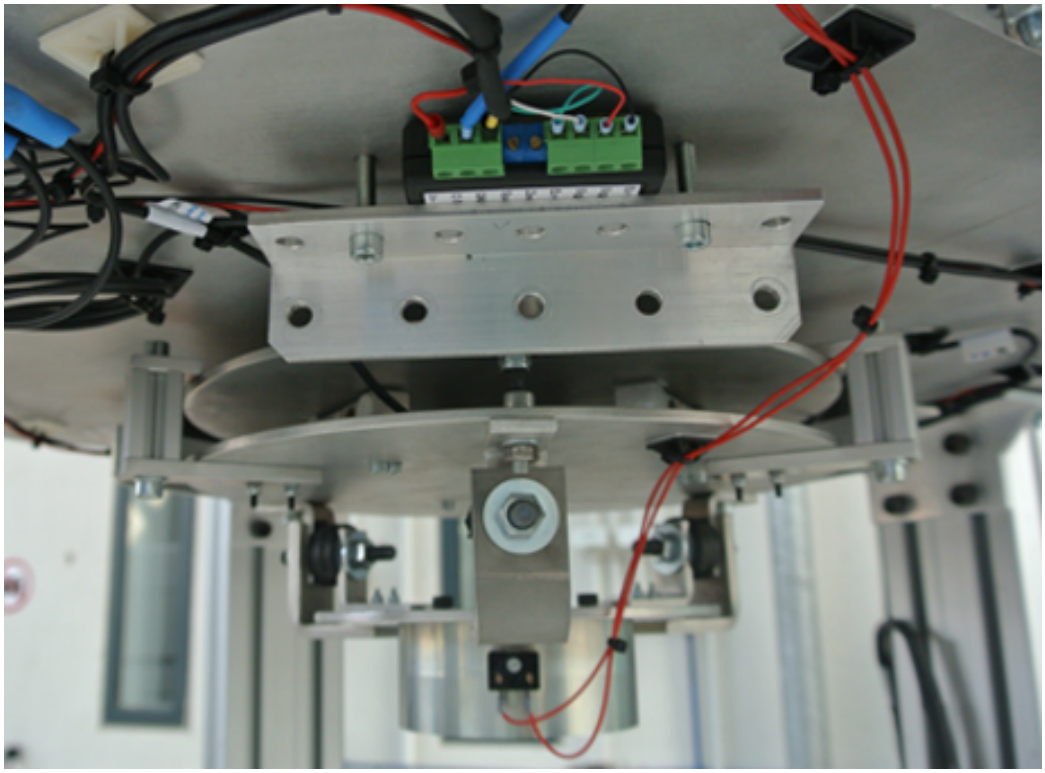

Fig. 2.8: SEC mounted in the ZARM capsule's upper platform

The entire subsystem mass is about 4.92 kg. The following table (Tab. 2.1) show the masses and dimensions of each component of the SEC system.

Component	**Mass [kg]**	**Dimension [mm]**
Cap	36.E-3	Φ122 x 27
Electromagnet	2,2	Φ100 x 43
Aluminium plate 1	0.245	Φ170 x 4
3 x L profile 1	46.8E-3	40 x 40 x 4
3 x Damper	0.105	Φ30 x 15
3 x L profile 2	43.8E-3	40 x 36 x 4
3 x Damper endpoint	0.402	48 x 55 x 6
Aluminium plate 2	0.663	Φ280 x 4
3 x Aluminium bar 1	70.8E-3	75 x 20 x 6
3 x Bosch^{TM} profile	58.2E-3	20 x 20 x 44
3 x Aluminium bar 2	42.6E-3	45 x 20 x 6
3 x Load cell	0.182	70 x 15 x 22
Aluminium plate 3	0.663	Φ280 x 4
Spacers, screws	0.162	-
Total	4,92	Φ318 x 115

Table 2.1: SEC component's masses and dimensions

2.1.1 Electromagnet, load cells and dampers features

This subsection contains a brief description of the features of the most important components of the SEC system which are:

- The electromagnet
- The load cells
- The dampers

The SEC was provided with an industrial electromagnet (Fig. 2.9).

Fig. 2.9: Electromagnet installed on the SEC

The electromagnet characteristics are shown in Tab. 2.2.

Voltage [V]	12
Power [W]	17
Current [A]	1.2
Coils	2350
Radius [mm]	50
Wire's thickness [mm]	0.5
Wire's length [m]	328
Coil's external radius [mm]	38
Coil's internal radius [mm]	25

Table 2.2: Electromagnet characteristics

Four different types of load cells have been studied for collecting the dynamic response of the SEC: three load cells for microgravity conditions and one for normal gravity.
All the load cells have the same dimensions (Tab. 2.1), and differ only in the maximum load (Fig. 2.10).

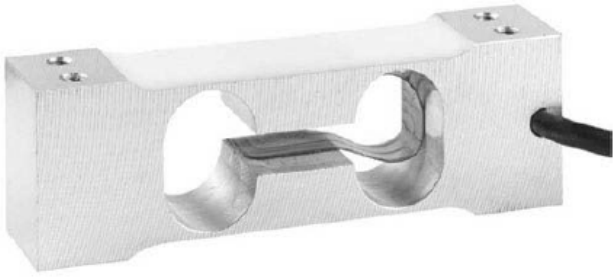

Fig. 2.10: Load cell

The property of the load cells are shown in Tab. 2.3.

	Microgravity		**Gravity**
	2 kg	**3 kg**	**5 kg**
Maximum load [N]	2g	3g	5g
Maximum warping [m]	4.E-4	4.E-4	4E-4
Excitation Voltage [V]	10	10	10
Sensitivity [mV/V]	2	2	2
Relative uncertainty	2.E-4	2.E-4	2.E-4

Table 2.3: Load cells characteristics

The load cell output was connected to a signal amplifier. Since the load cell output signal used very low voltages, the distance between the load cells and the amplifiers has been reduced as much as possible in order to minimize the thermal noise in the cables, the power dispersion and other electromagnetic disturbances.
The damping properties of the SEC system are provided by the action of three shear dampers (Fig. 2.11).

Fig. 2.11: Damper

During the design process of the SEC two different type of dampers were considered, both type with the same dimension (Tab. 2.11).

	Type 1	**Type 2**
Maximum load [N]	80	110
Maximum warping [m]	2.5E-3	2.5E-3

Table 2.4: Dampers characteristics

During the microgravity test campaign the 3 kg shear beam load cells and the type 2 dampers were installed on the SEC. The reason of this choice will be explain in section 2.2.

2.2 Dynamic Analysis

To study the feasibility of the proposed technology, a series of dynamic analyses had been performed with computational software:

- the electromagnet sphere of influence and attraction
- the dynamics of the tethered system to the target
- the response of the target after the probe impact

In the following subsections particular focus will be given to the SEC response after the probe impact, analyzing the step of design process of the load acquisition system and the simulation of the response of the SEC to the impact with the probe. The other two object of the dynamic analyses will be briefly described. The Matlab script for the dynamic simulation can be divided into four main step:

- 1^{st} step, electromagnet's force and sphere of influence simulation. The electromagnetic attraction forces acting on the ferromagnetic probe has been obtained simulating the electromagnet with a software called Finite Element Method Magnetics (FEMM). FEMM showed that the influence of the electromagnet was no longer relevant after 10 cm, for this reason, the magnetic field of the electromagnet has been analyzed (axial symmetric analysis) from 10 cm to 0 cm (contact with the electromagnet). In order to completely discretize the forces generated by the electromagnet in the proximity of its attraction surface, an array of 10 cm x 10 cm has been filled with the forces obtained with FEMM software around the electromagnet itself with an accuracy of 1 mm.
- 2^{nd} step, time optimization

  A subroutine has been written after the magnetic field analysis to determine the launch time from SEC to GUN, considering the two variables *probe's impact velocity* and the *distance between SEC and GUN*. The calculations showed that the optimal travel time was around 1.5 s.

- 3^{rd} step, probe weight

  An important point was the precision of the launch, which could be lowered by disturbances due to the tether. The tether dynamics could affect the trajectory of the probe, with the risk of it missing the electromagnet. These disturbances had a stronger effect on low-mass probes. To estimate the precision of the launch the disturbances has been considered as an initial velocity along the Y direction, calculated as a fraction of the velocity on the X-axis (probe motion axis). The effect of the disturbances has been considered with probe of different masses (Tab. 2.5).

Probe mass [kg]	**Min Disturbance** $\frac{v_y}{v_x}$	**Max Disturbance** $\frac{v_y}{v_x}$
0.1	0.1	0.3
0.2	0.1	0.3
0.5	0.1	0.3

Table 2.5: Probe masses and tether disturbances

  Analyzing these disturbances (as described in the fourth step), a range of distances from approximately 340 to 410 mm has been chosen as the optimal distance between the SEC and the GUN, because it guaranteed a higher probability of success, as the disturbances did not change the trajectory significantly.

- dynamic simulation

  The dynamic simulation was a linearized simulation evaluating the forces during the entire probe trajectory with a two-dimensional interpolation method, calculating the next accelerations, velocities and positions. The calculation lasts until the probe arrives in contact with the electromagnet positioned in $x = 0$. The progresses have been evaluated plotting the x and y-position in the function of time and constructing an x-y plot in order to evaluate the choice of the alternatives given by the different masses. It is important to highlight that the trajectories graphs show that higher masses are less perturbed; nevertheless higher masses need a stronger magnetic field because of the

higher inertia. The conclusions of this dynamic simulation gave three important results:

- The choice of probe mass in order to understand the best weight
- The distance between GUN and SEC in order to have the best chance to hit the target
- The evaluation of the tether deployment

Analysing the assumptions made for the percentage perturbation and after observing the probe's trajectory progress, it was clear that the 500 g mass was the best probe, as it could travel farthest. Nevertheless, a mass compromise of approximately 200 g was selected as the best choice to have a greater attraction from the electromagnet point of view, because the probe inertia was less relevant. To show the reason of this choice, the following graphs analyze the trajectories of the three masses with the same disturbance percentage (Fig. 2.12 - Fig. 2.13 - Fig. 2.14). The red lines in the graphs represent the projection of the electromagnet: if the trajectory of the probe goes outside the red lines at X = 0, the probe will miss the SEC. Each group of three lines represent the trajectories of the probe, starting from several distances: 30 cm, 40 cm, 50 cm, 60 cm (top to bottom in the graph). The attracting electromagnet is on the left side of the each graph; the trajectories start from the GUN, on the far right.

LEGEND

- Dashed blue line: 100 g mass
- Continue magenta line: 200 g mass
- Dot-dash black line: 500 g mass

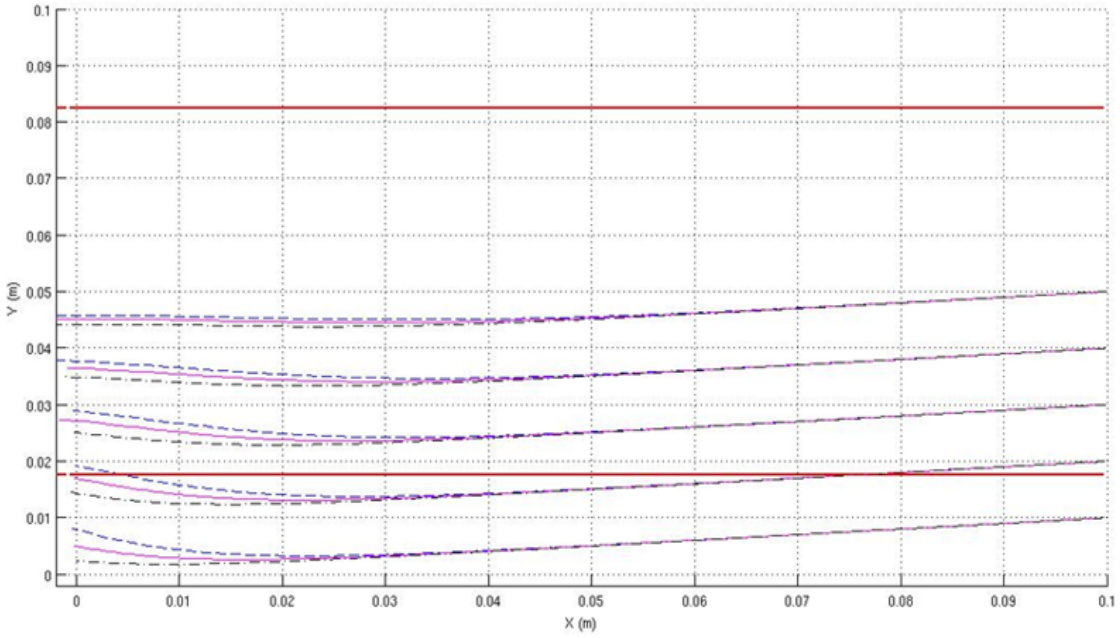

Fig. 2.12: 10% disturbance

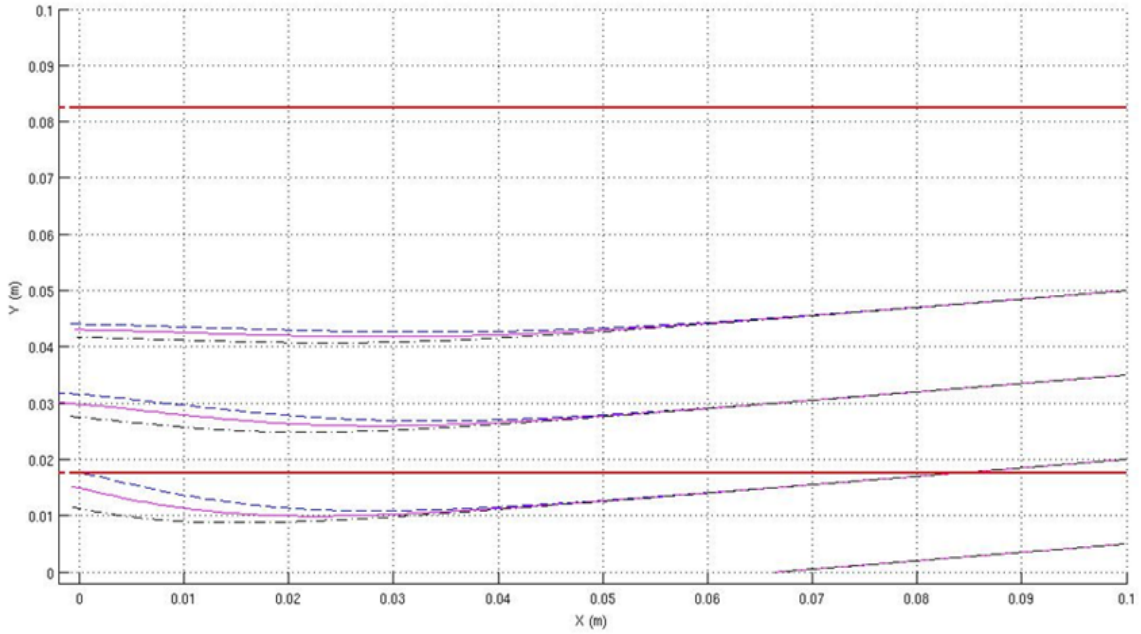

Fig. 2.13: 20% disturbance

The analysis showed also that the optimal distance between the SEC

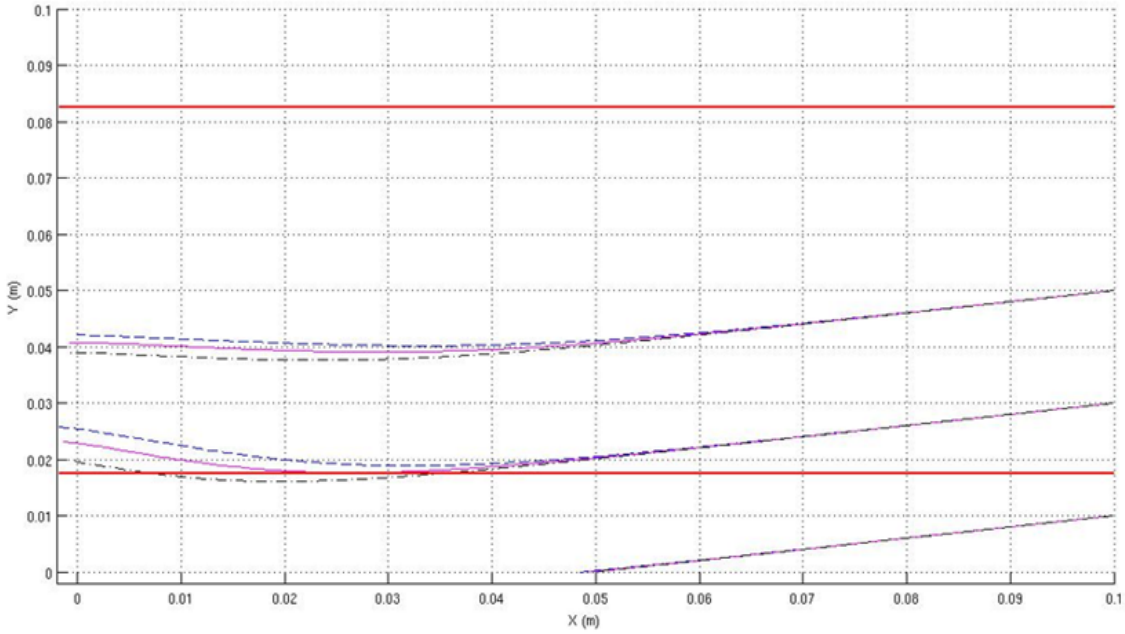

Fig. 2.14: 30% disturbance

and the GUN laid in the 340 - 410 mm range.

2.2.1 Impact model and load cell choice

The system is composed of an electromagnet and two identical 4 mm thick aluminium plates. The external plate can be considered fixed. Three load cells link them together, and the second platform is linked to the electromagnet by three shear dampers. Considering the system configuration, to design the SEC an impact model consisting in a simplified vibrating system made of three masses, three stiffness elements and two damping elements has been used (Fig. 2.15):

- m_1 represents the mass of all the elements located between the electromagnet and the dampers (0.41 kg)
- m_2 represents the mass of the electromagnet (2.2 kg)
- m_3 represents the mass of the ferromagnetic probe (0.218 kg)

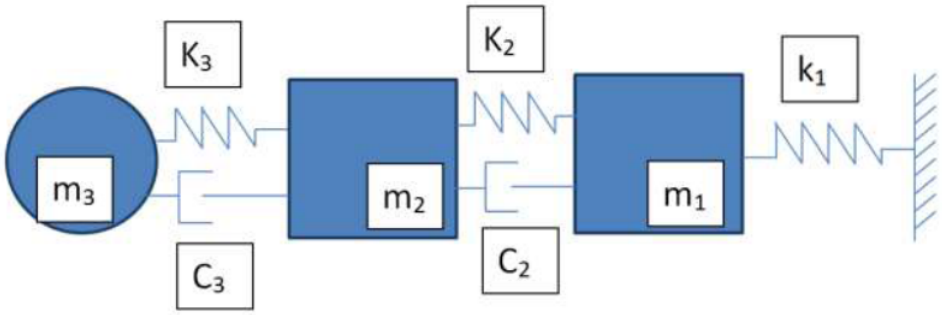

Fig. 2.15: Elastic system model

A Matlab script that simulates the complete vibrating system has been written. The simulation lasts for the whole 4.7 seconds of free fall between the drop and the impact with the ground on the bottom of the drop tower. The model of the impact in the complete simulation is slightly more complicated than the one used to dimension the load cells, and includes the mass of the sphere in the equation. The initial condition of the simulation is the velocity of the sphere towards the electromagnet before the impact. The motions equations are the following:

$$m_1\ddot{x}_1 + 3c_2\dot{x}_1 + 3(k_1 + k_2)x_1 = 3c_2\dot{x}_2 + 3k_2x_2$$

$$m_2\ddot{x}_2 + (3c_2 + c_3)\dot{x}_2 + 3(k_2 + k_3)x_2 = 3c_2\dot{x}_1 + 3k_2x_1 + c_3\dot{x}_3 + k_3x_3$$

$$m_3\ddot{x}_3 + c_3\dot{x}_3 + k_3x_1 = c\dot{x}_1 + k_3x_2$$

In this system of equations $\dot{x}_3 = v_{i,s}$ (initial velocity of the sphere before the impact with the electromagnet) has been taken as initial condition. The system overall mass, including the supports, load cells, dampers and the three masses, is about 3 kg and the load cells are considered to be perfectly elastic and have no damping component c. The load cells data-sheet reported the maximum load and maximum warping of this sensor: their elastic constant has been estimated equal to the ratio of these two parameters provided by the manufacturer.
The dampers have both an elastic constant, which has been calculated in the

same way of the elastic constant of the load cells, and a damping coefficient c. The value of this parameter has been determined inverting the following equation $\xi = \frac{c}{2\sqrt{mk}}$, and assuming that the damping factor of the dampers (natural rubber) is equal to 0.5 [8]($\xi = 0.5$) (Tab. 2.6).
In other to keep a large safety margin, c has been underestimated considering that the parameter m in the last equation represents for every coefficient c the mass of the moving part of the system; to define the c_2 component a mass $m = m_2 + m_3$ was used, while to define the c_3 component a mass $m = m_3$ was utilized.

	Load cells			**Dampers**	
	2 kg	**3 kg**	**5 kg**	**Type 1**	**Type 2**
Max. load [N]	19.62	29.43	49.05	80	110
Max warp. [m]	4.e-4	4.E-4	4.E-4	2.5E-3	2.5E-3
Elastic const. [Nm-1]	4.905E+4	7.358E+4	1.226E+5	8.083E+6	1.111E+7
Damping coeff. [Nsm-1]	-	-	-	4.46E+3	5.23E+3

Table 2.6: Elastic and damping constant of the load cells and dampers

The elastic and damping components between the sphere and the electromagnet at the moment of impact, k_3 and c_3, have been accurately defined; the damping component was calculated with the equation $\xi = \frac{c}{2\sqrt{mk}}$ with $\xi = 0.0023$ (steel damping coefficient), with k defined as follow. The electromagnet-sphere elastic constant was firstly evaluated as a hardness level on the Brinell scale.
The Brinell hardness number is obtained by dividing the applied force, P, expressed in kg, by the actual surface area of the indentation which, is a segment of a sphere as illustrated in (Fig. 2.16).

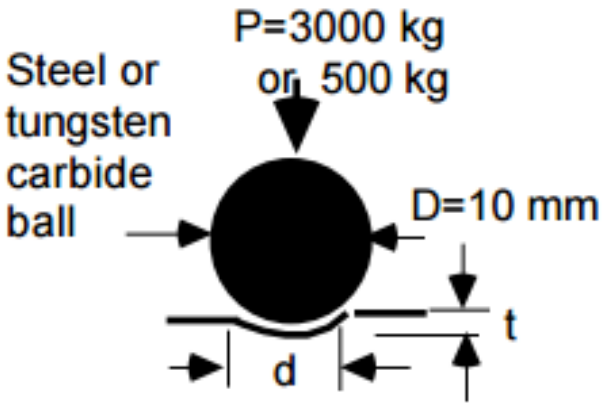

Fig. 2.16: Brinell tester

The Brinell hardness is evaluated with the following formula:

$$HB = \frac{P}{\pi D t} = \frac{2P}{\pi D[D - \sqrt{D^2 - d^2}]}$$

The parameter in the equation are:

- P, apllied force in kg
- D, diameter of the identer in mm
- t, surface indentation depth in mm
- d, diameter of the indentation at the surface in mm

The Brinell scale characterizes the indentation hardness of materials through the scale of penetration of an indenter, loaded on a material test-piece. For evaluating k_3 the values of HB = 120, 150, 170, 200 were considered extracting the surface indentation depth t and dividing the applied load P to t:

$$k_3 = \frac{P}{t}$$

Considering P = 3000 kg and D = 10 mm the value of t and k_3 and consequently c_3 are (Tab. 2.7):

	HB = 120	**HB = 150**	**HB = 170**	**HB = 200**
t [mm]	0.796	0.637	0.562	0.477
k_3 [Nm-1]	3.7E+7	4.62E+7	5.24E+7	6.17E+4
c_3 [Nsm-1]	43.9	49.05	52.24	56.68

Table 2.7: Value of t, k_3 and c_3

Considering the electromagnet response as a hardness level on the Brinell scale, the maximum load exerted by the electromagnet on the probe at the impact and the impact time has been estimated (Tab. 2.8).

Travel [m]		**HB = 120**	**HB = 150**	**HB = 170**	**HB = 200**
0.41	Load [N]	4514	5047	5373	5827
	Time [s]	2.3E-4	2.E-4	1.9E-4	1.8E-4
0.34	Load [N]	5698	6371	6782	7357
	Time [s]	2.3E-4	2.E-4	1.9E-4	1.8E-4

Table 2.8: Loads and times of impact in function of HB

Since it was not safe to assume that the value of the elastic constant obtained with the Brinell coefficient, and also the value of the damping component was exactly correct, a further verification has been conducted, exploiting the laws of mechanics.
When an impact occurs it has two edge cases, represented by a completely elastic shock with energy conservation and a totally inelastic impact with a complete energy loss. Modeling the problem in the two edge cases it has been possible to find a range of value for both the elastic and damping coefficient of the impact, assuming that any realistic impulsive force was lower than a completely elastic impact, but typically higher than a wholly inelastic one. In order to obtain accurate measurements in realistic conditions, the load cells were chosen to make sure that the operating range of these sensors included the forces both in the elastic and inelastic case. The two impact cases were modeled considering the velocity of the electromagnet after the impact with the sphere. As no external forces act on the system, the angular momentum

Q must be preserved.
For the inelastic impact the electromagnet velocity has been calculated as:

$$v_e = \frac{v_s m_s}{m_s + m_e}$$

The elastic impact preserves the total mechanical energy as well as the angular momentum. Considering the system of the two equation of conservation the extracted final velocities are:

$$v_{s,f} = \frac{(m_e - m_s)v_{s,i}}{m_s + m_e}$$

$$v_e = \frac{2m_s v_{s,i}}{m_s + m_e}$$

The parameters in the above formula are respectively:

- m_e electromagnet mass
- m_s sphere mass
- v_s sphere velocity (inelastic impact)
- v_e electromagnet velocity
- $v_{s,i}$ sphere initial velocity (elastic impact)
- $v_{s,f}$ sphere final velocity

The vibrating system includes the electromagnet and the structure and has the velocity of the electromagnet (in one of the two cases) as an initial condition. It's important to note that in the inelastic case the mass of the sphere must be added to the mass of the electromagnet, as these two elements are joined.
With this considerations the system can be simplified to this (Fig. 2.17):

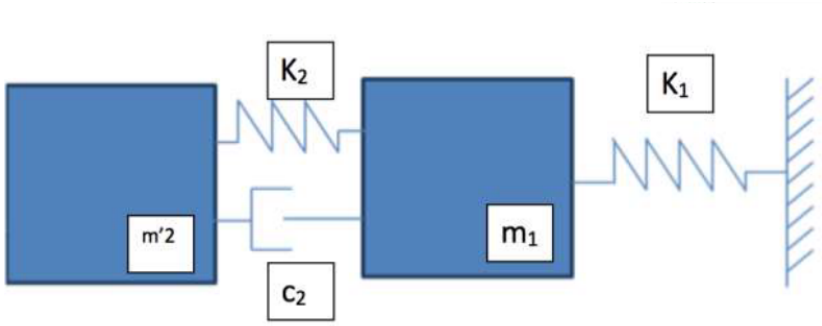

Fig. 2.17: Two masses elastic model

The simplified system's motion equations can be written as:

$$m_1\ddot{x_1} + 3c_2\dot{x_1} + 3(k_1 + k_2)x_1 = 3c_2\dot{x_2} + 3k_2x_2$$

$$m_2'\ddot{x_2} + 3c_2\dot{x_2} + 3k_2x_2 = 3c_2\dot{x_1} + 3k_2x_1$$

A Matlab script that simulates the system in the two impact cases has been written, inserting the elastic and damping constant of the load cells and dampers as previously defined. The computational simulation showed that the impact was closed to an elastic one when using the constants estimated with the Brinell Hardness (HB = 200) and $\xi = 0.0023$, confirming that the first hypothesis to simulate the shock of the probe on the electromagnet was correct.

2.2.2 Load cells and dampers dimensioning

An orbital docking mechanism should guarantee loads on both vehicles as low as possible, with low vibration frequencies and short damping period of the load acting on the target vehicle. For this reason, during the development process of the target interface, a damping system has been designed in order to absorb the impact forces and transmit little load as possible to the structure in which it is mounted. On the other hand FELDs is not just only a technology demonstrator, since another objective of the test campaign has been to measure and evaluate the impact forces' evolution; for this reason

the loads transmitted by the dampers to the structure need to be in the operating range of the shear beam load cells. The load measurement system has to be able to hold the weight of the entire SEC in ground conditions with ground gravity in order to reduce the damping time of the oscillations generated by the transition from 1g gravity to microgravity as low as possible. The dampers and load cells' choice takes all these parameters into account. Since the weight force on the load cells was around 30 N ($m_1 + m_2 + m_3$), they needed to support that load avoiding overdimensioning. The choice of the eligible load cells has been between nominal loads of 1 2 and 3 kg. As each rigid load cell need rigid damper to transmit stronger vibrations the choice of the dampers is instrumental to exploit the entire operating range of the load cells, and the rigidity of the dampers has been calculated accordingly to the load cells operating range. Nevertheless rigid dampers bring a higher oscillation frequency and damping time of the target system. During the design process of this subsystem it has been also considered that overdimensioning the load cells would have caused a loss of precision in the impact force measurements; the system would also have been distant from a realistic docking setup, lowering the value of the technology demonstration. The following step of the design process of the SEC system was to evaluate if the chosen load cells could accurately measure the impact forces. The following graphs show, for the two types of impact, the warping of the load cells (as a percentage of the maximum warping) as a function of time before and after the impact (Fig. 2.18 - Fig. 2.19 - Fig. 2.20). The first simulation were conducted considering the least rigid dampers available (P = 30 N, warping = 5 mm) in order to reduce the frequency of the impact response.

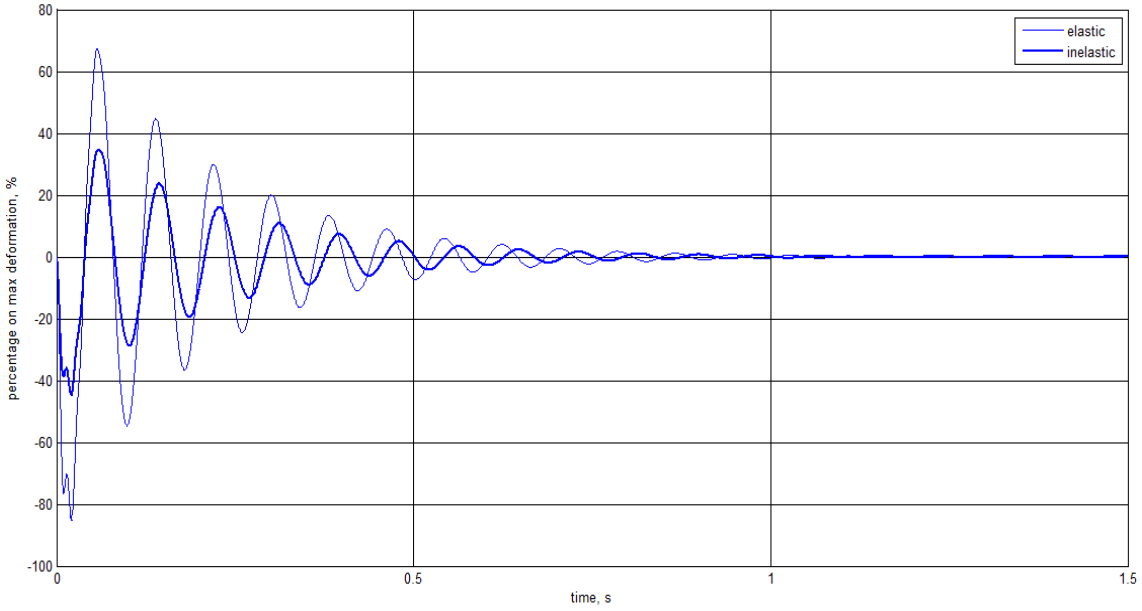

Fig. 2.18: 1 kg load cell, 0.4 mm warping

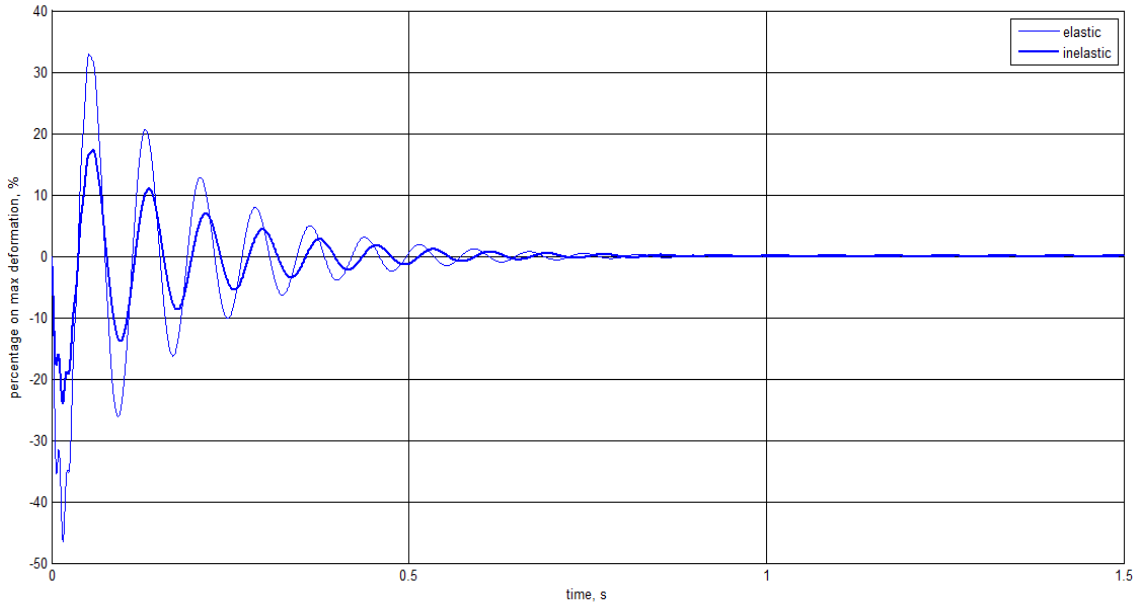

Fig. 2.19: 2 kg load cell, 0.4 mm warping

Since the precision of the load cell is 0.1% of the maximum nominal load, the 3 kg cells presents evidently a bigger error. The 1 kg cells had the issue that they were not ideal to ground conditions since they wrapped by

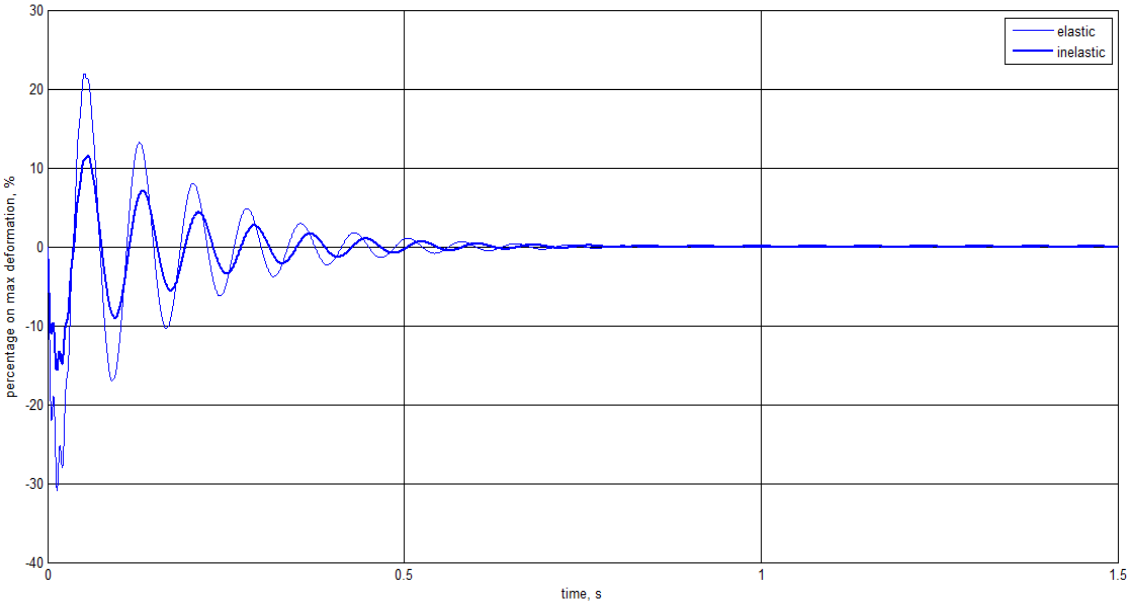

Fig. 2.20: 3 kg load cell, 0.4 mm warping

100% only supporting the entire structure weight without further load. This considerable warping would have cause oscillations in microgravity conditions thus affecting the impact load measurements. For this reason only the 2 and 3 kg load cell (Fig 2.21 - Fig. 2.22 - Fig. 2.23 - Fig. 2.24) were considered eligible to fly in the test campaign: they have the same nominal warping of 0.4 mm and the same dimensions of 70 mm x 22 mm x 15 mm. The dampers coupled to the load cells had a higher rigidity than the first considered, in order to allow the transmission of higher load to the structure and to use the load cells fully.

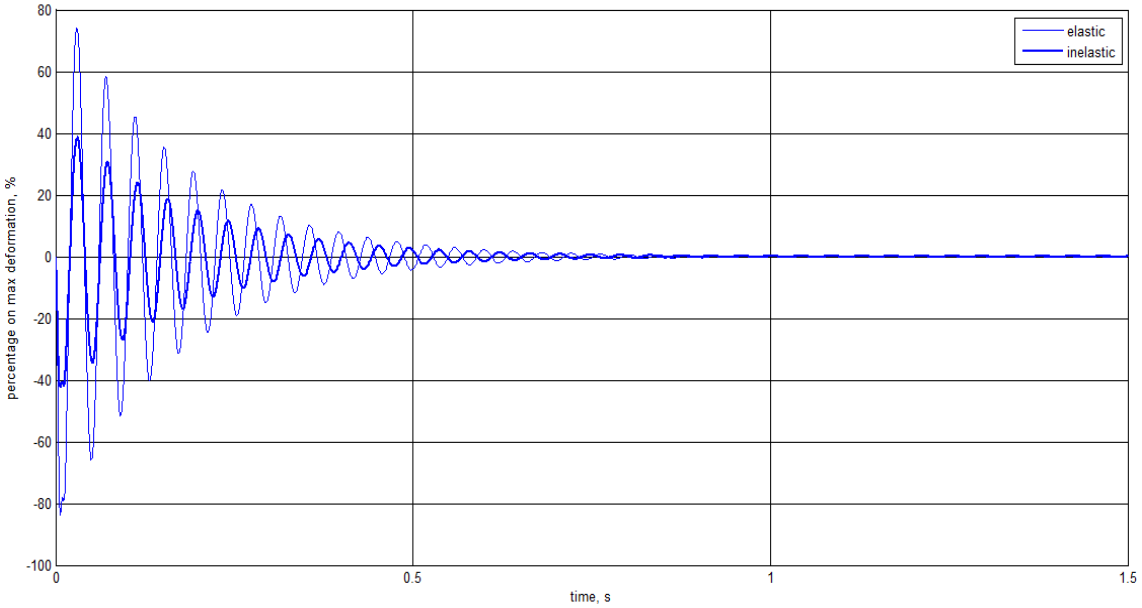

Fig. 2.21: 2 kg load cell, 80 N damper

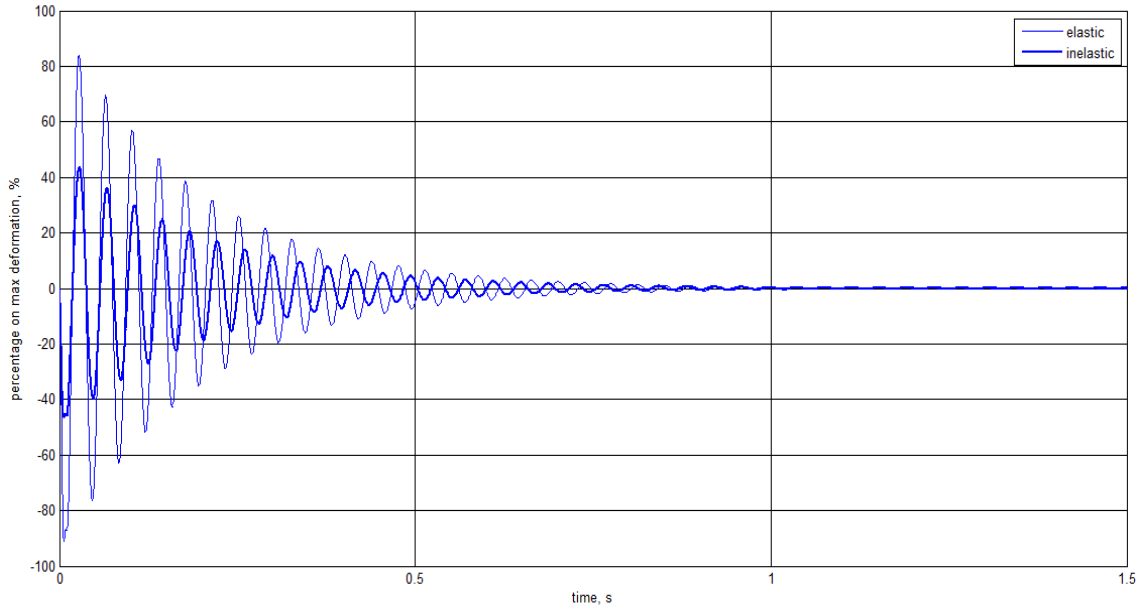

Fig. 2.22: 2 kg load cell, 110 N damper

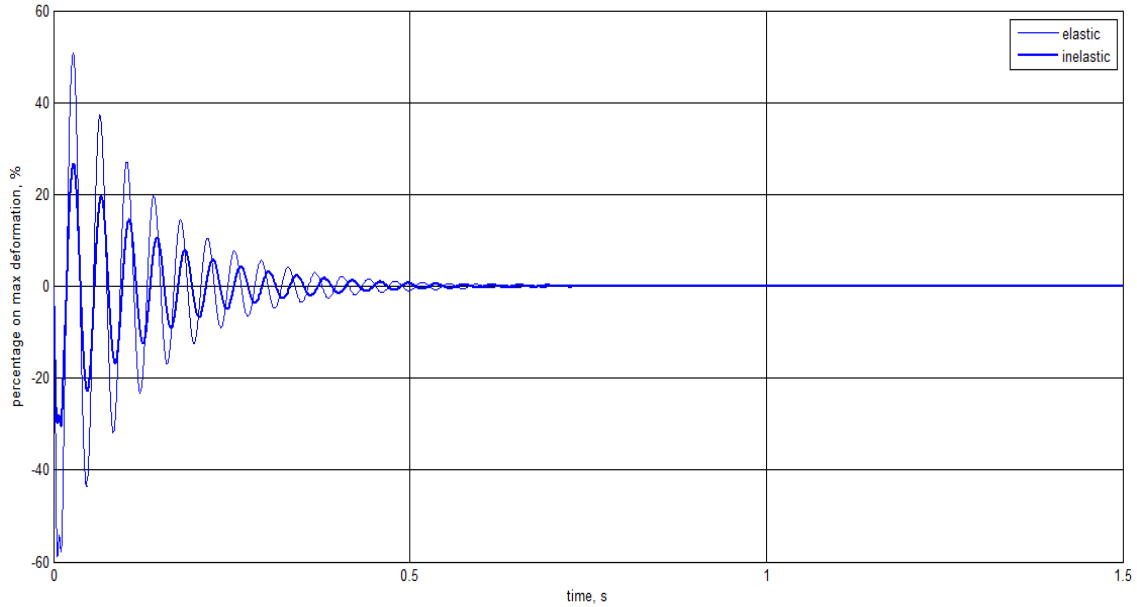

Fig. 2.23: 3 kg load cell, 80 N damper

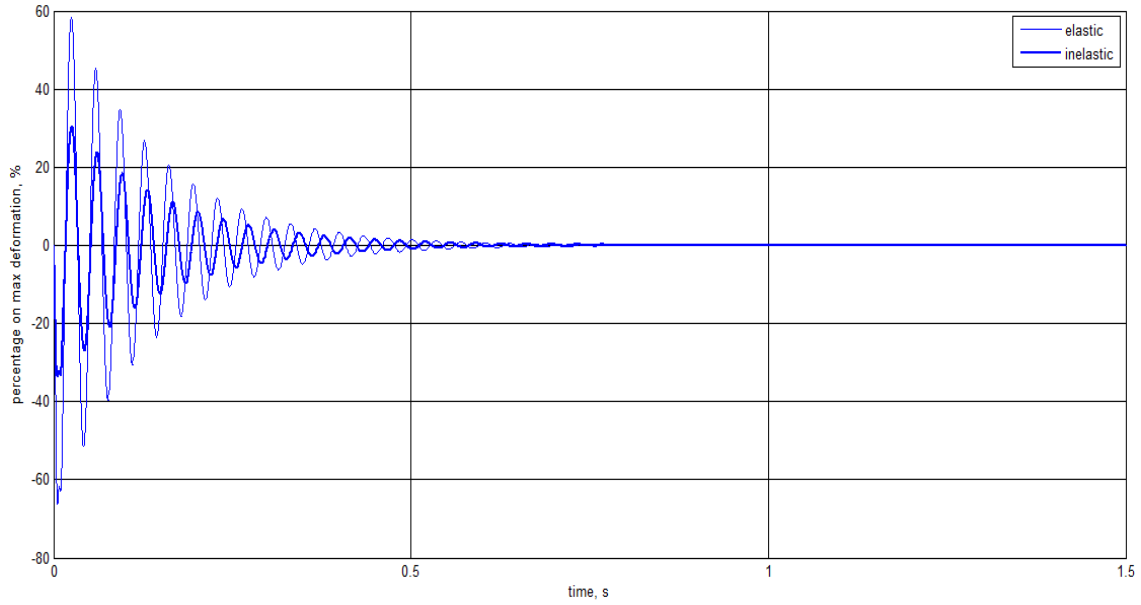

Fig. 2.24: 3 kg load cell, 110 N damper

Fig. 2.25 and Fig. 2.26 show the load cell warping as a function of time: the sudden absence of gravity at the beginning of the drop phase, the impact and the moment before the final deceleration at the end of the drop phase can be noticed.

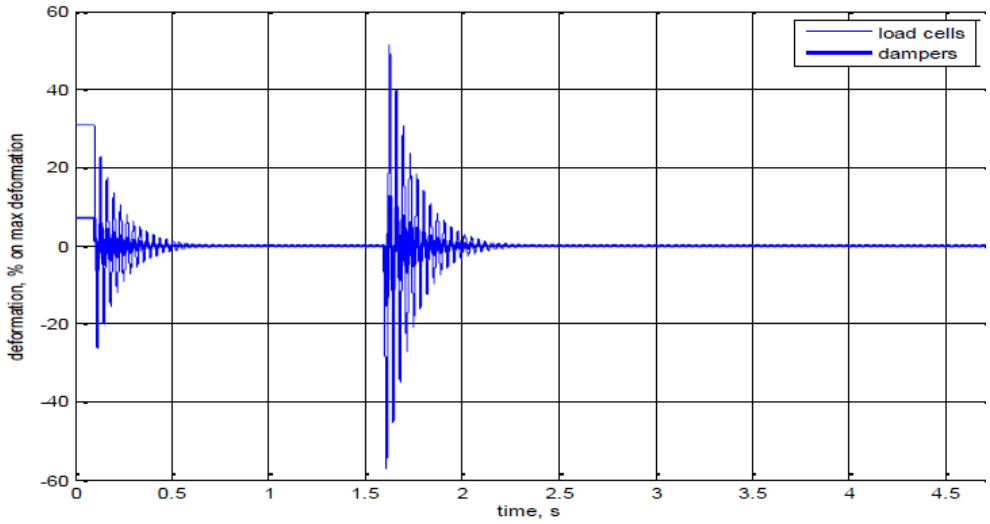

Fig. 2.25: 2 kg load cell and damper warping

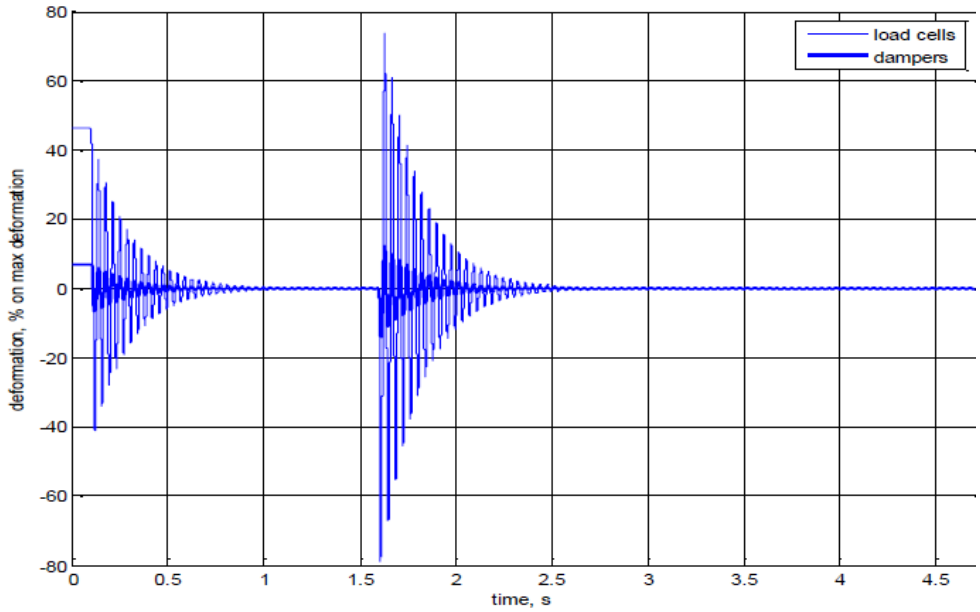

Fig. 2.26: 3 kg load cell and damper warping

The final deceleration is not measured by the load cells since the rigid end point described earlier limit their warping. Further accurate studies has been conducted, estimating a load on a single load cell around 15 N (halving the first load estimate). The following graphs show the dynamic load trend on the load cells and on the dampers for both the configuration with the 2 kg load cells (Fig. 2.27 - Fig. 2.28) and the configuration with the 3kg load cells (Fig. 2.29 - Fig. 2.30) estimated with the numerical simulations.

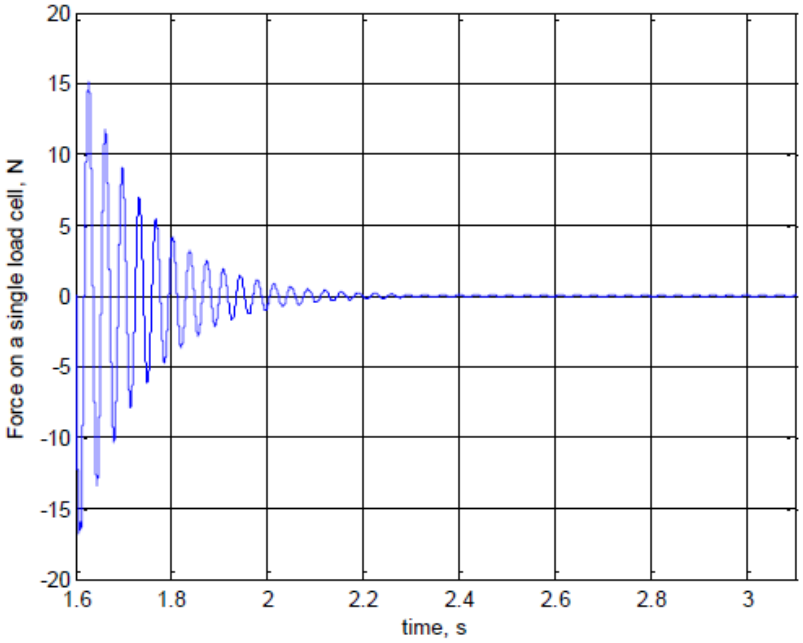

Fig. 2.27: 2 kg load cells' dynamic load trend

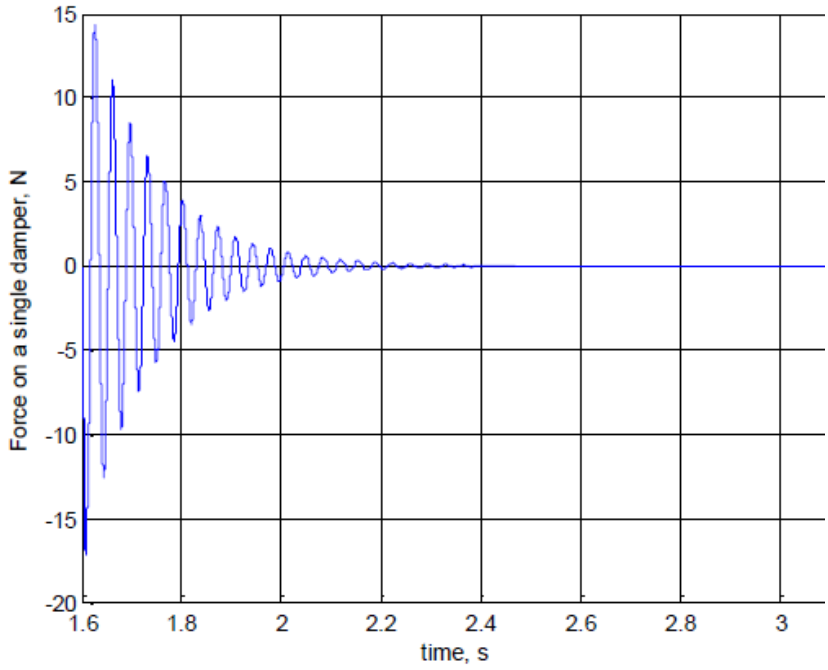

Fig. 2.28: Dampers' dynamic load trend

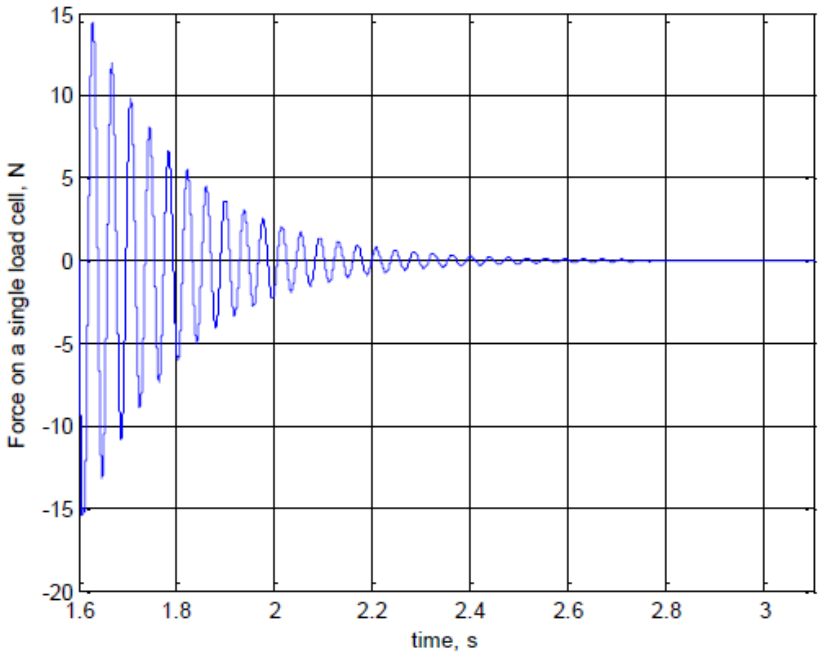

Fig. 2.29: 3 kg load cells' dynamic load trend

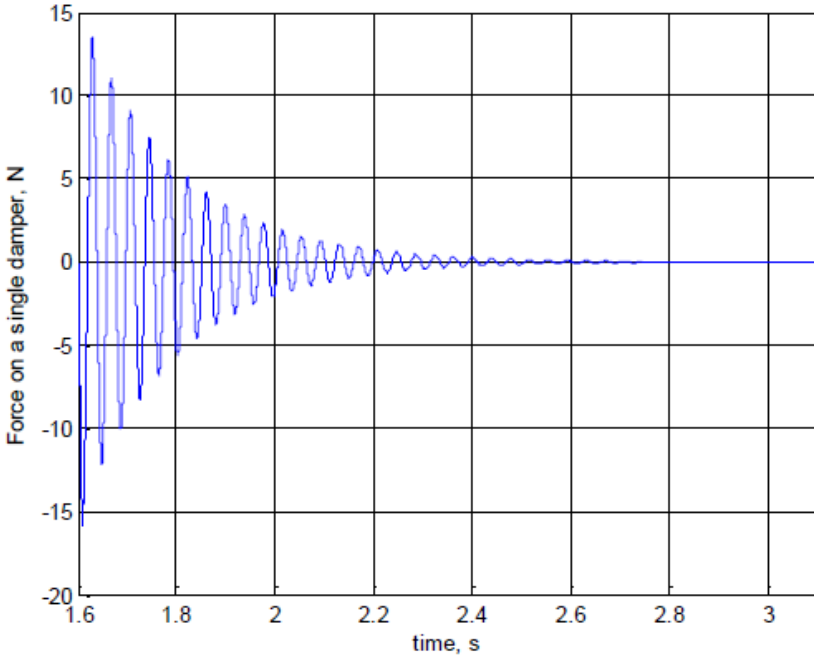

Fig. 2.30: Dampers' dynamic load trend

During the test campaign the 3 kg has been employed to make sure that the load cells could cover the impact force (in case of stronger impact than the expected one from the simulations). The frequency response of the system, obtained with the numerical simulation, show a peak around 25 Hz and become negligible for frequencies above 100 Hz (Fig. 2.31).

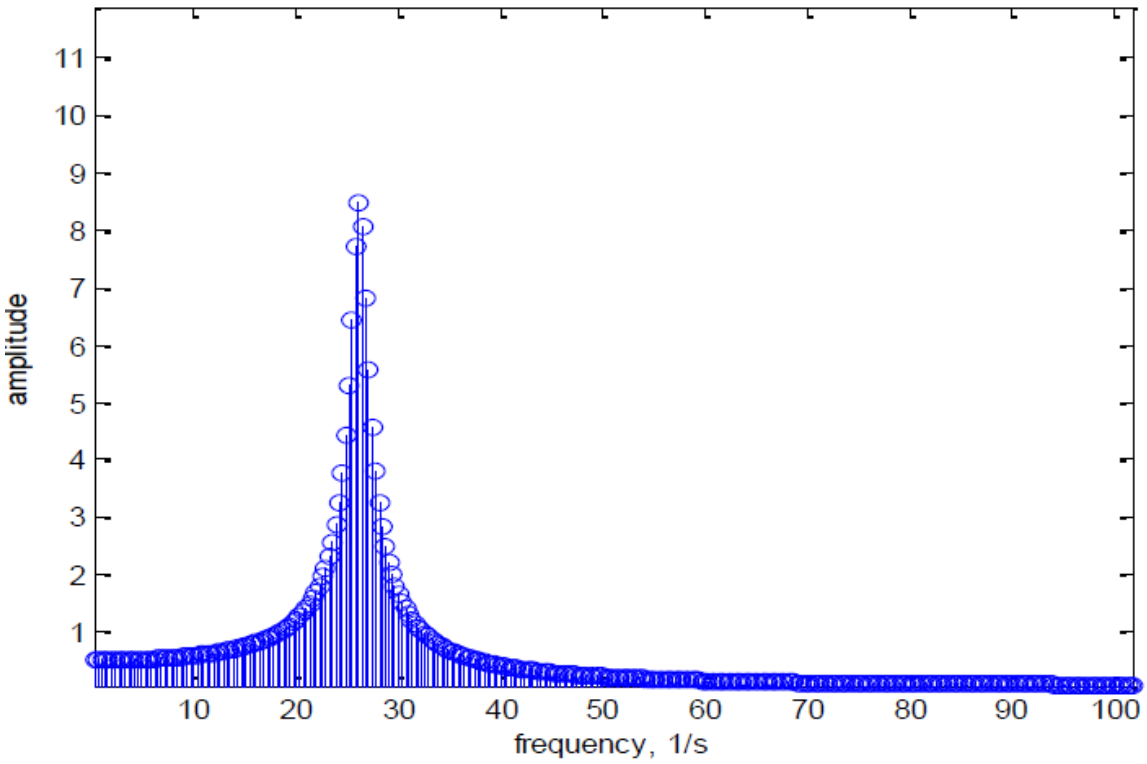

Fig. 2.31: Frequency response of the system

2.3 Structural load simulation

One of the key aspect of the design process of the target subsystem was to conceive a structure which could both simulate the behavior of a real spacecraft docking target interface, and support the heavy loads due to the capsule landing in the deceleration chamber. During the deceleration phase the capsule is subjected to a 50g deceleration, and consequently each components that fits in the capsule must bear the loads which arise from its own inertia. For this reason a finite-element analysis was performed with ANSYS, considering the worst-case load in every critical components. Two types of analysis were conducted: a linear static one, and a non linear static one, to verify if there was some cause of non linearity (large displacement and material non linearity) in the model. The results obtained in the two analyzes were identical, therefore only the results referring to the linear one are reported (Fig. 2.32 - Fig. 2.33 - Fig. 2.34 - Fig. 2.35 - Fig. 2.36 - Fig. 2.37). After analyzing the results related to the finite element analysis the 6082 aluminium alloy was selected to realize the various components of the system, as its yield stress leaves an ample safety margins over the expected equivalent stresses.

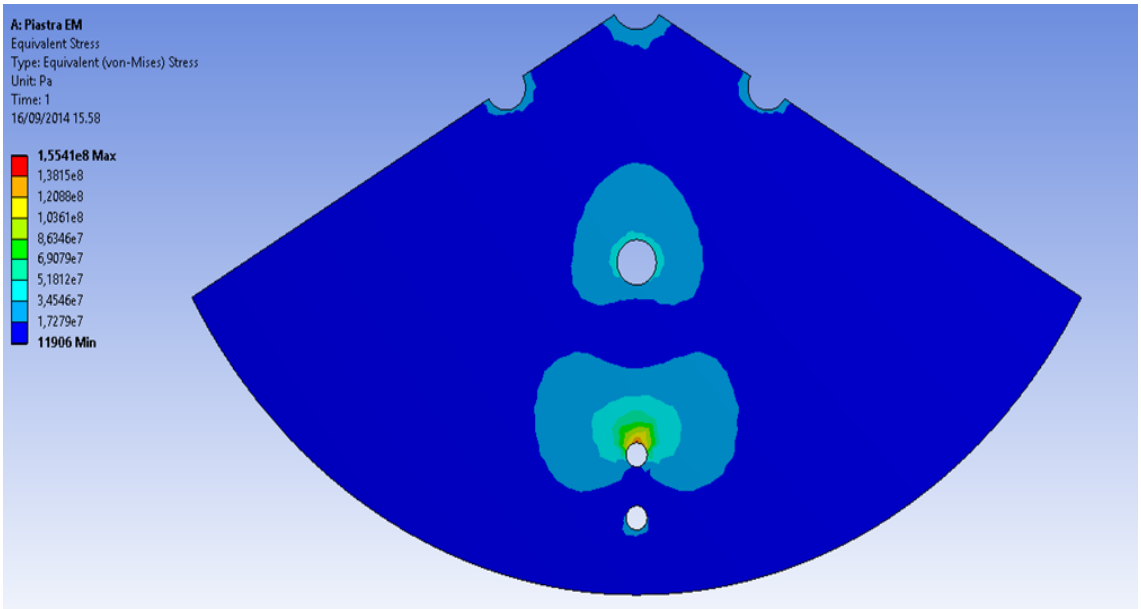

Fig. 2.32: Load on SEC aluminum plate 1

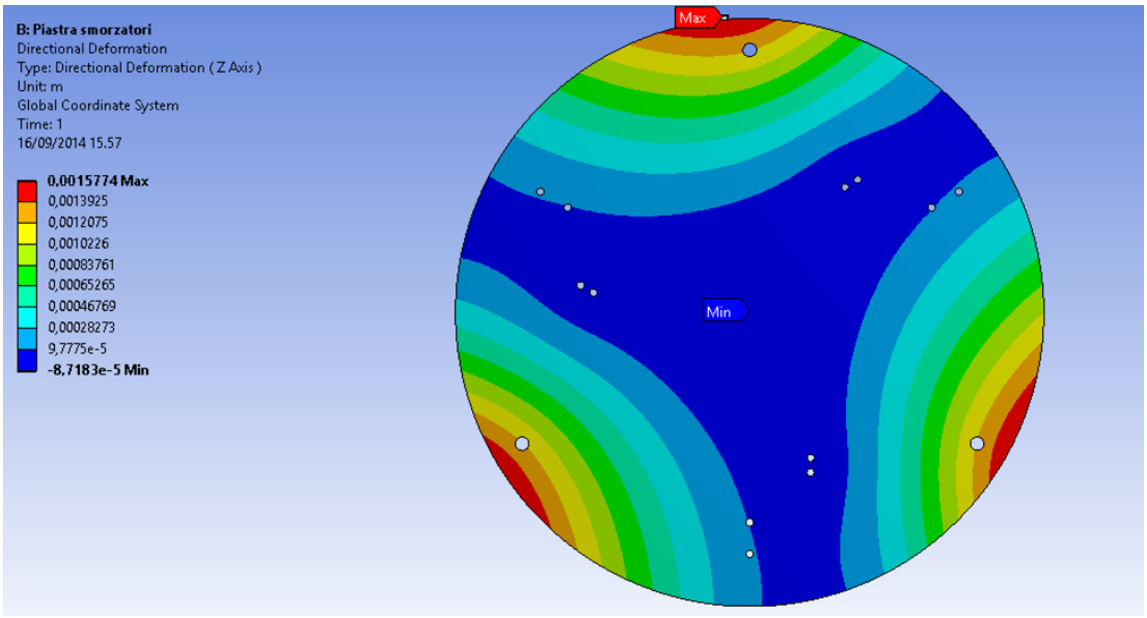

Fig. 2.33: Load on SEC aluminum plate 2

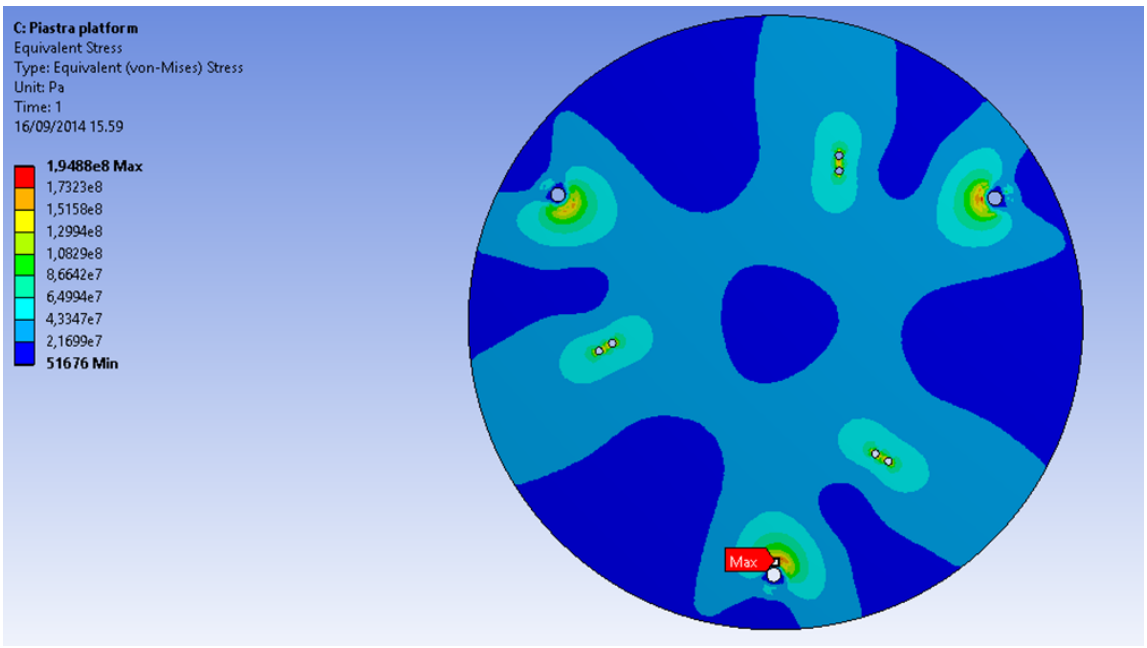

Fig. 2.34: Load on SEC aluminum plate 3

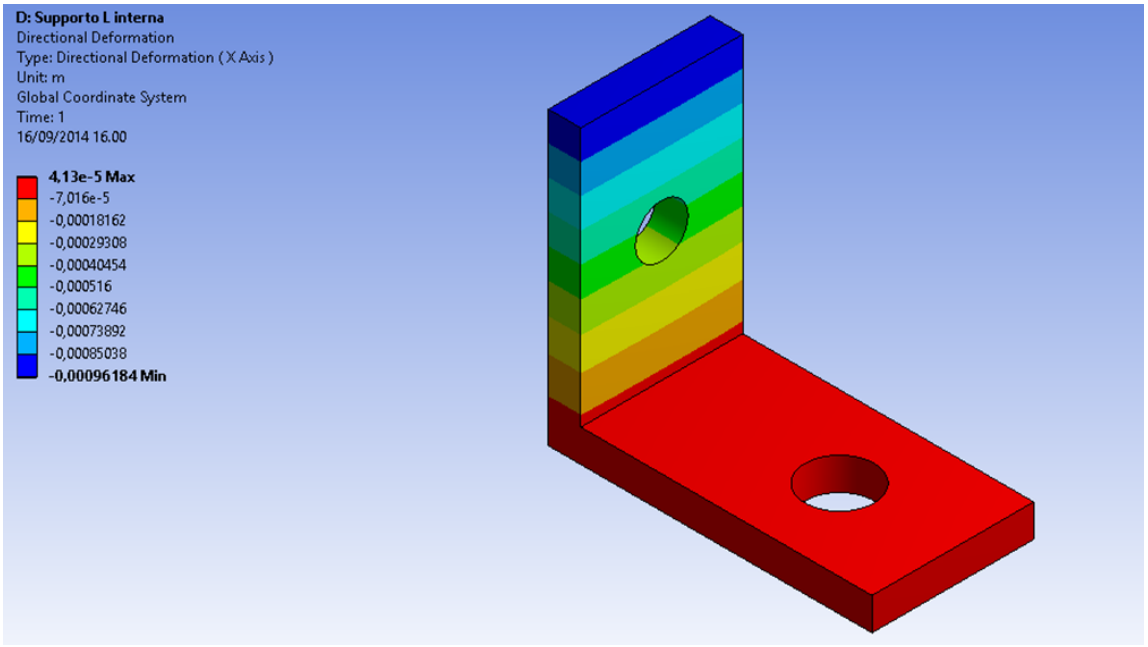

Fig. 2.35: Deformation on the L profile between aluminum plate 2 and the dampers

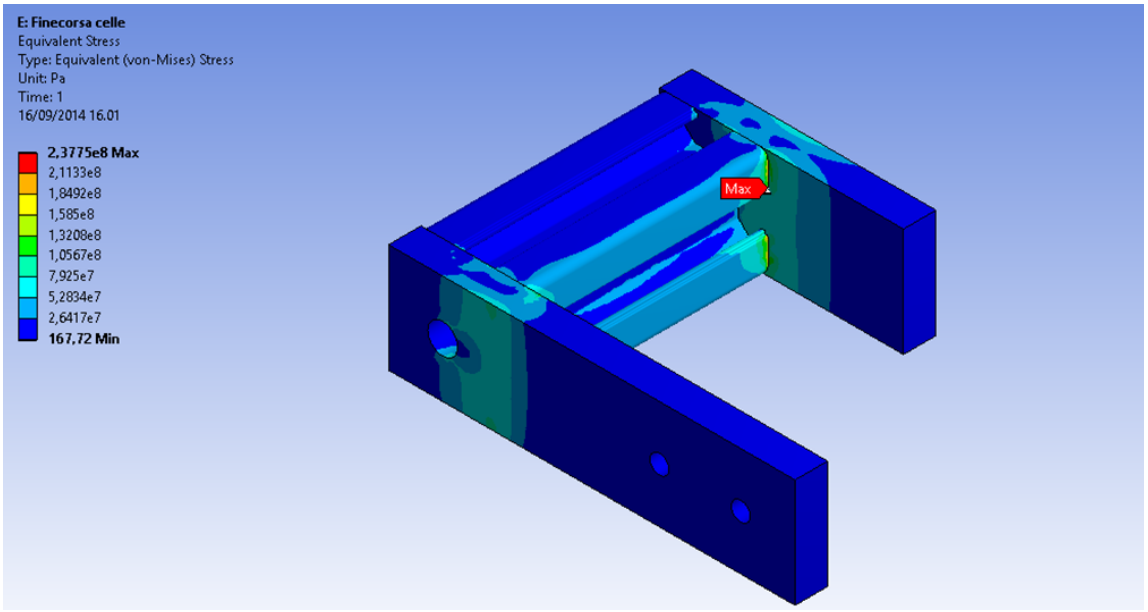

Fig. 2.36: Load on shear beam load cells endpoint

The unique components that have been realized with a different material were the shear dampers endpoint, which have been built with C40 steel, since they had to withstand a much higher load.

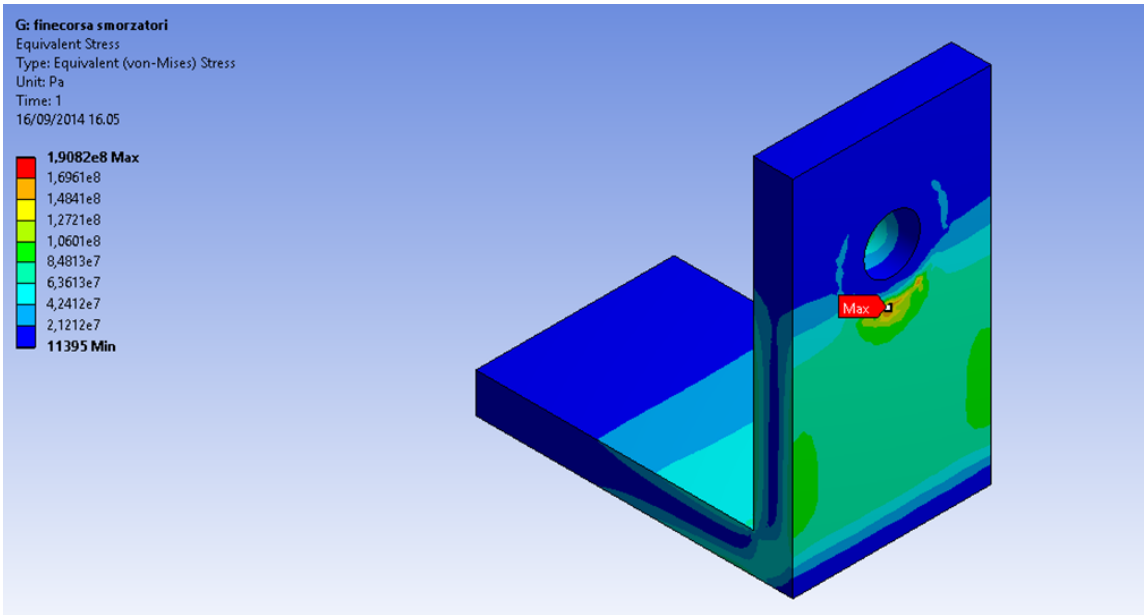

Fig. 2.37: Load on shear dampers endpoint

Chapter 3

GUN system

The GUN system represents the experiment launch unit and is composed by a spring and an aluminium structure in order to achieve the correct spring compression for the docking simulation (Fig. 3.1).

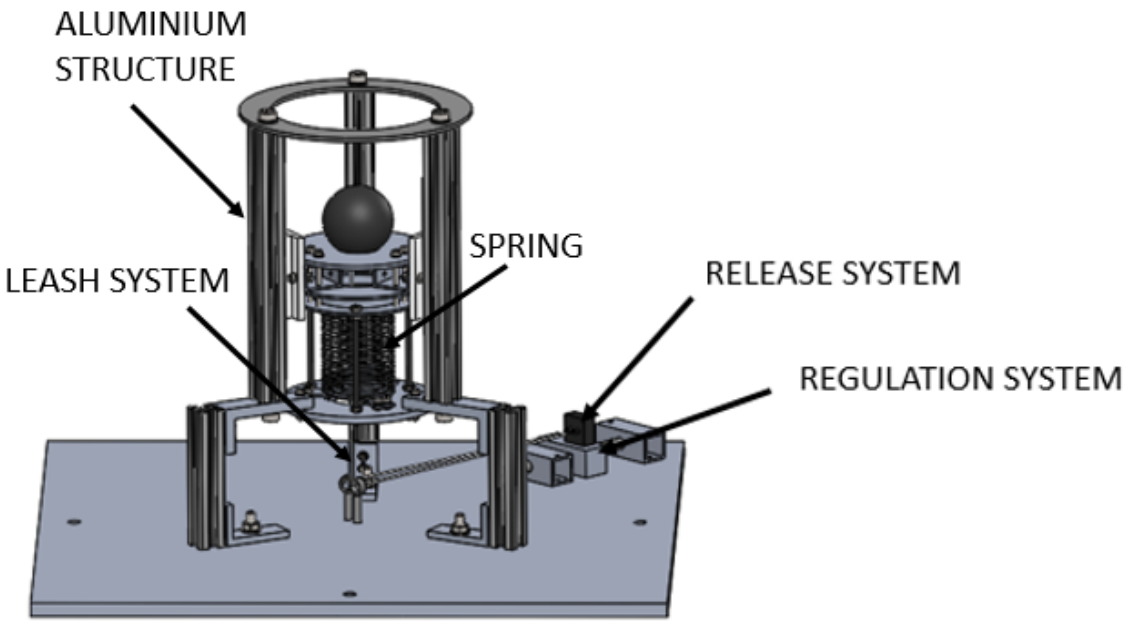

Fig. 3.1: GUN system

The Leash system is one of the two subsystems which are integrated into the GUN, and consists in the set of a kapton wire, (also called tether), and a ferromagnetic sphere (probe) that are connected together. The other

subsystem that is integrated in the launch unit is the Regulation/Release system, which has the role to keep the tether tense before the shot and to allow and almost impulsive shot when the docking has to be performed.

3.1 Mechanical description

The aluminium supporting structure has been designed in order to withstand the structural loads due to the capsule's deceleration phase and to minimize the friction during the shot of the probe. Starting from the bottom, three L profiles are arranged at 120 degrees and are mounted in the lower capsule platform with three M6 screws. This three aluminium components are connected to one Bosch^{TM} profiles each by two aligned M3 screws. The profiles has the role to support the entire weight of the system (Fig. 3.2).

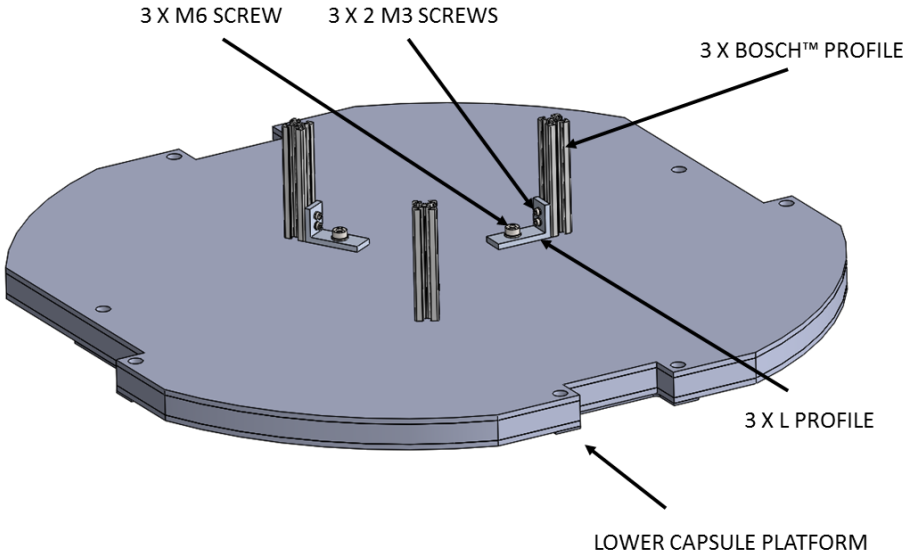

Fig. 3.2: GUN mounting on Capsule platform

Three others aluminium L profiles are mounted with two aligned M3 screws each to the Bosch^{TM} profiles. These L profiles support the GUN itself

and are connected to the base of the GUN which consists in an aluminium disk with a hole in the middle in order to allow the tether to pass (Fig. 3.3).

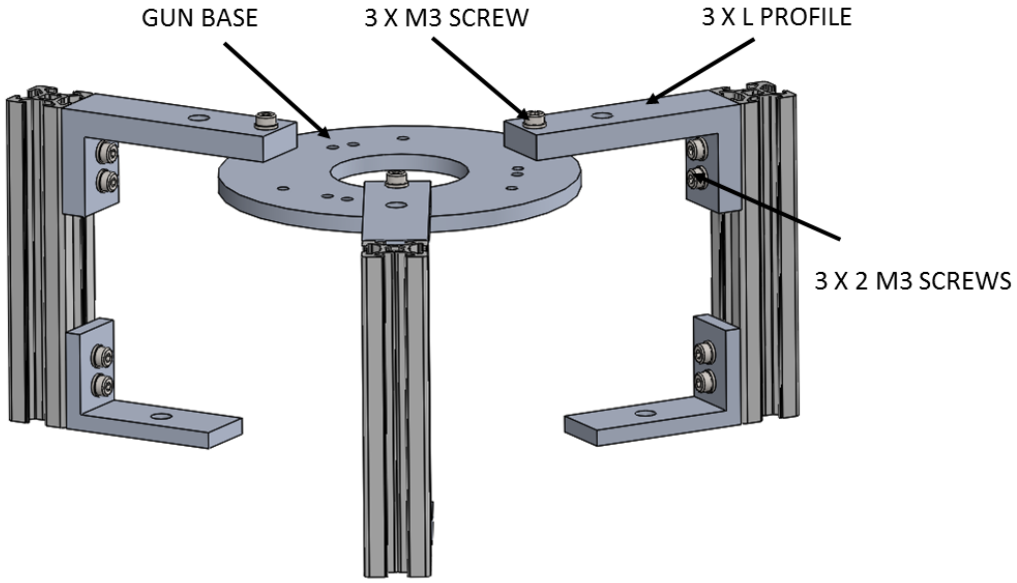

Fig. 3.3: GUN base

The lower side of the spring is attached to the GUN base with three aluminium blocks, mounted on the base with two aligned M3 screws each (Fig. 3.4). The upper side of the spring touches an aluminium disk (1). The diameter of aluminium disk 1 is equal to the diameter of the base of the GUN in order to allow the spring's compression and the motion of the tether. There is another aluminium disk (2) with the same diameter of and parallel to aluminium disk 1: between these two disks three rectangular aluminum profiles are placed in order to house the Teflon^{TM} guides. Each aluminium rectangular profile is fixed to the two discs with two aligned M3 screws, and the guides are integrated on each rectangular profile with other two aligned M3 screws. The set of aluminium disk 1, aluminium disk 2, Teflon^{TM} guides and the rectangular profiles is called *Ring*.

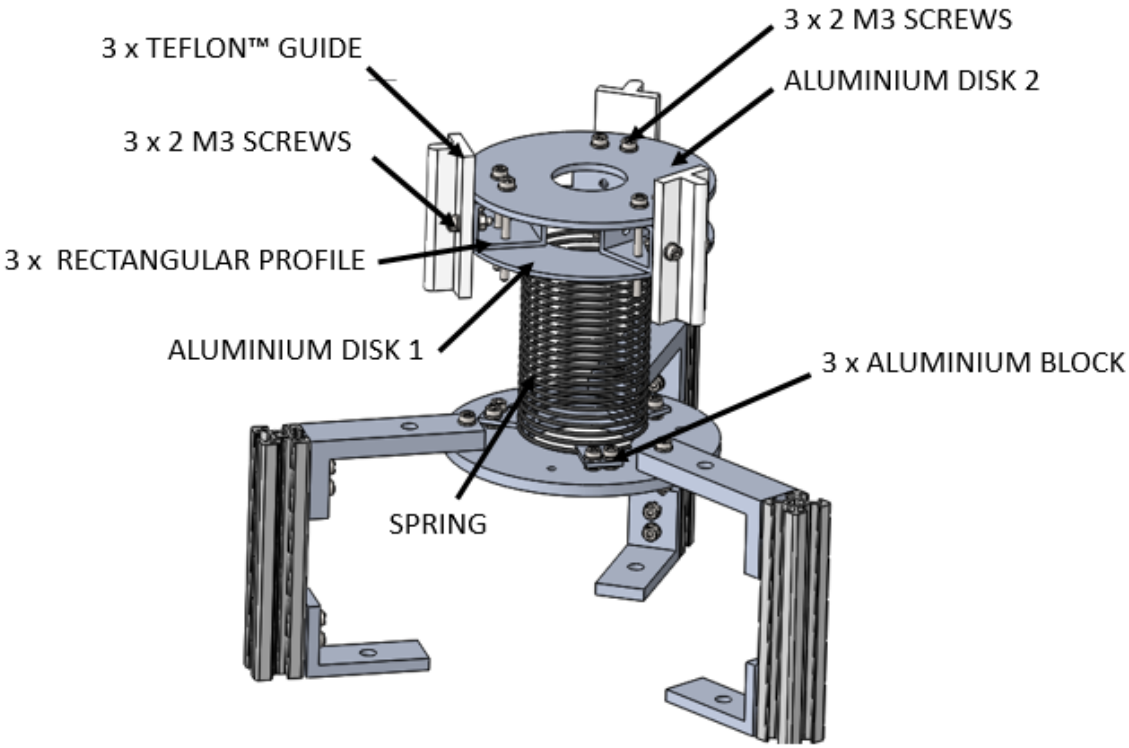

Fig. 3.4: Mounting of spring and guides

The guides slide inside three 20 mm x 20 mm Bosch^{TM} profile providing the proper alignment with negligible friction (Fig. 3.5). The first idea to obtain the correct alignment and spring's decompression consisted in exploiting a Plexiglass^{TM} cylinder with an internal diameter equal to the diameter circumscribed by the guides, but after an extensive laboratory test campaign this solution was discarded because of the friction that was being formed. Since the entire system should have integrated in the ZARM capsule in gravity condition, but the tests were performed in microgravity condition, the "flight" spring was not strong enough to hold the wire tense during the system's preparation for the tests. For this reason an aluminium disk, supported by three M4 threaded rod, was mounted to hold the weight of all the components above the spring before each Drop. The height of the spring support could be regulated, accordingly to the required spring compression,

just acting on the nuts of the threaded rods.

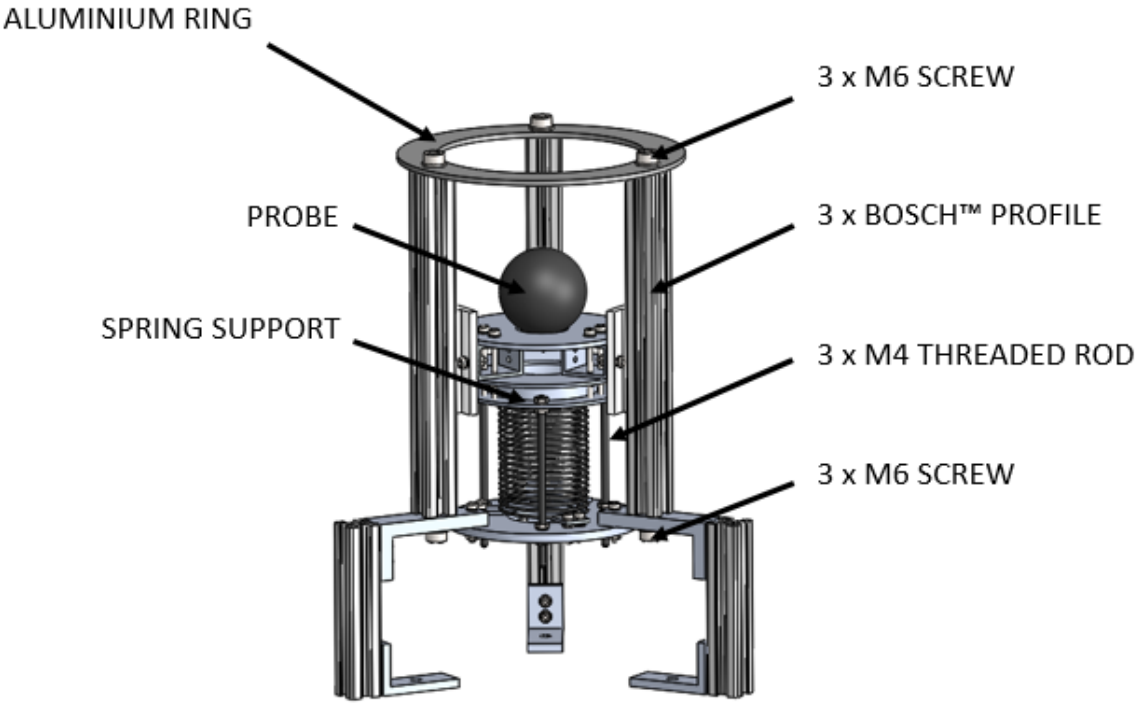

Fig. 3.5: GUN

The probe is a ferromagnetic spherical shell with a thickness of 3 mm and a diameter of 50 mm, designed to realize the docking thanks to the electromagnet attractive force. The shape has been chosen spherical because it can connect the SEC regardless of the approach angle. When the tether is kept tense the probe leans on aluminum disk 2. The wire is attached to the probe from one side and to the GUN from the other, and was taken longer than the minimum distance between the SEC and the GUN to leave a margin of safety in case of imperfect trajectory and to ensure the docking performance. Since the distance between the GUN and the SEC was set to 340 for the first four drop and to 410 mm in the last drop, the probe has to fly respectively for 290 or 360 mm (the distance minus its radius): for this reason a safety margin of more then ten centimeters was taken, using a 550 mm long tether.

As explained before the guides slide inside the grooves of the profiles. These

profiles are 200 mm long (longer than the spring travel to avoid the spring from blocking) and are mounted at 120 degrees on the GUN base's L profile with one M6 screw each in the lower side, while in the upper side they are connected to an aluminium ring by three M6 screws arranged at 120 degrees. When the spring support is regulated accordingly to the spring compression needed, the tether is stretched from one side by the probe block on aluminium disk 2 and from the other side by the Release system; the first configuration of this system (pre-campaign configuration) consists in an electrical connector with a 20 mm long constantan wire which burns at the instant of the shot beginning, by applying a peak of current of 40 A (Fig. 3.6 - Fig. 3.7). When the constantan burns, the tether is released and the spring decompressed, thus allowing the probe to move towards the electromagnet.

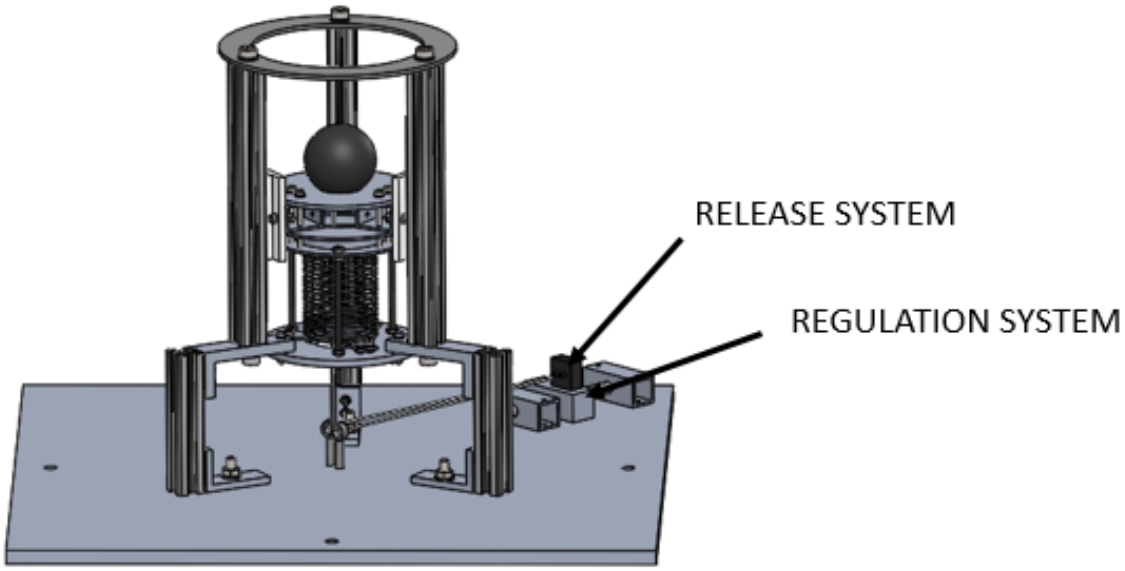

Fig. 3.6: Release and Regulation system

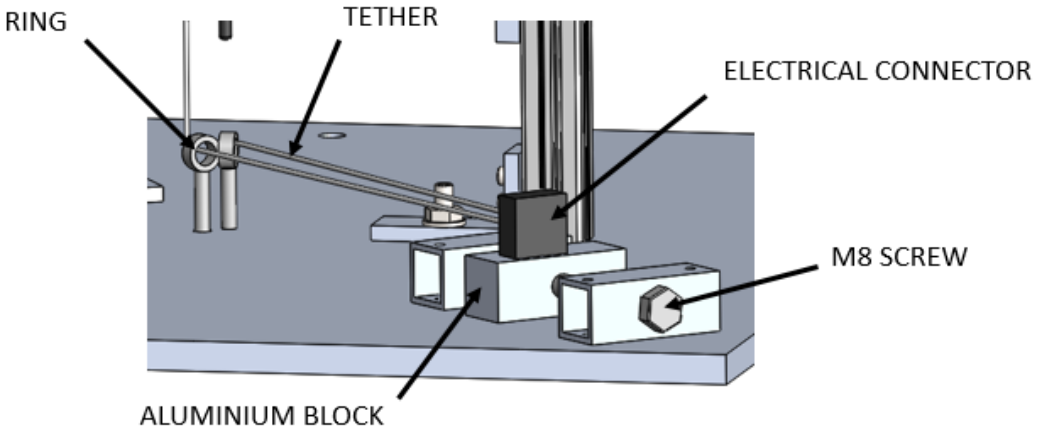

Fig. 3.7: Release and Regulation system, zoomed view

In Fig. 3.7 is possible to see a zoomed view of this two systems. One hand of the tether is connected to the probe, while the other is tied to a ring at the base of the GUN. In order to guide the tether deployment after the release, another ring is placed near the previous ring. The tether is kept tense by the costantan wire forming a U shape around it. Since a little portion of the tether is in touch with the constantan wire, this must be insulated from the heat generated by the short circuit with an adhesive aluminum foil. The electrical connector with the constantan wire is mounted in a Regulation system, consisting in an aluminum block with a threaded hole which moves back and forward thanks to the rotation of an M8 threaded rod. This system has been designed to regulate the tension of the tether just acting on the rod, avoiding the use of an automatic actuator. When the constantan wire burns, the tether is instantaneously released and the spring decompressed, giving to the probe the desired momentum. The first configuration of the Release system was changed in Bremen from the one planned before the campaign. In particular, two components were added:

- a torsion spring between the constantan wire and the clamp in order to make the tether release smoother (Fig. 3.8).
- a cylindrical plexiglass tube between the clamp and the screw in the middle of the GUN to act as a guide for the tether (Fig. 3.9).

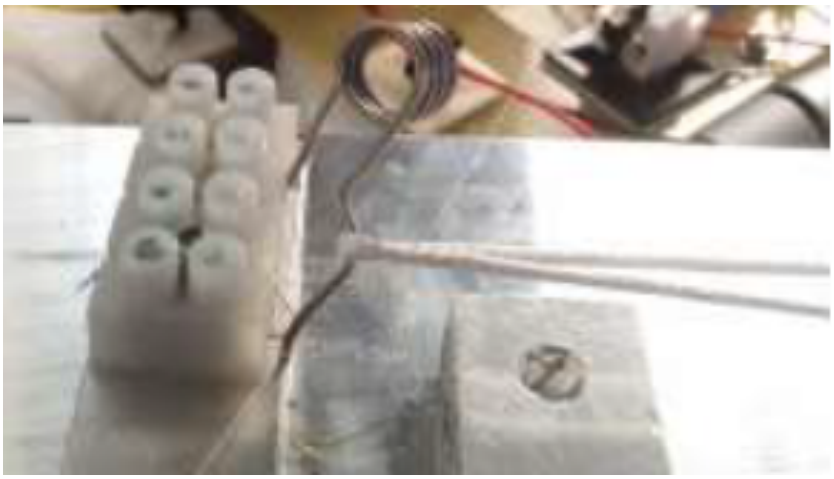

Fig. 3.8: Torsion spring

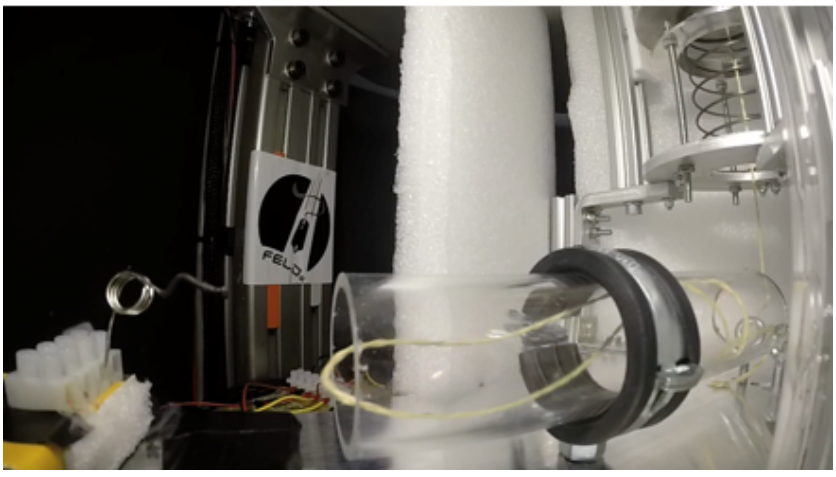

Fig. 3.9: Plexiglass tube

The idea behind the torsion spring is to have an immediate tether release after the constantan burn without it getting stuck or folding the tether. One end of the spring is blocked by the clamp and the other spring's end is inserted inside the constantan wire, which is also blocked by the clamp. The tether is inserted behind the torsion spring. Immediately after the constantan burns, the torsion spring is released; the tether release is smooth and extremely fast. During some tests with the release system using the torsion spring, it

has been noticed that the tether, after the release, often slammed against the GUN, so a tube was inserted to avoid the tether getting snagged on the GUN supports. The entire GUN system was integrated in the lower platform of the ZARM capsule by three M6 screws at 120 degrees which connect the platform and the supporting structure (Fig. 3.10 - Fig. 3.11). Between the supporting structure and the platform three adjustable length spacers were inserted, in order to perform tilted shot.

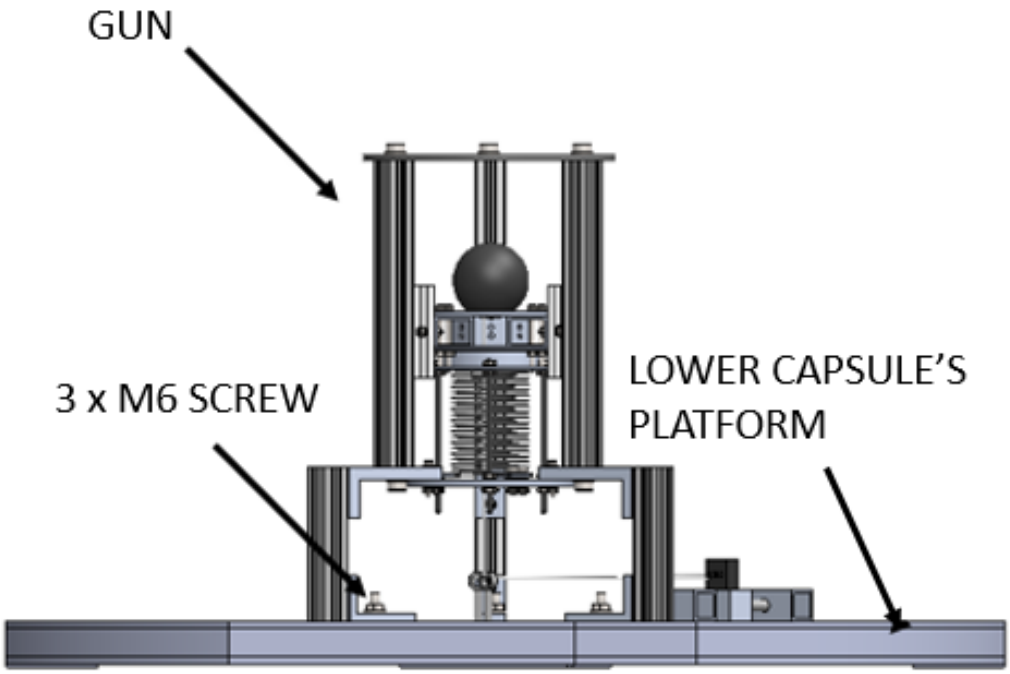

Fig. 3.10: GUN mounted on ZARM lower capsule's platform, rendering

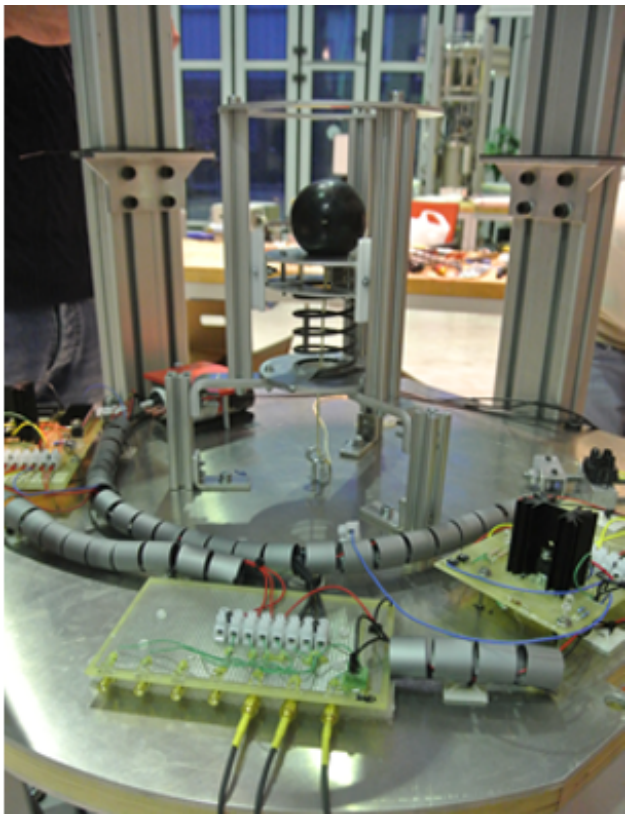

Fig. 3.11: GUN mounted on ZARM lower capsule's platform

The entire subsystem mass is about 1.118 kg. The following table (Tab. 3.1) show the masses and dimensions of each component of the GUN system.

Component	**Mass [kg]**	**Dimension[mm]**
3 x L profile 1	58.63E-3	50 x 30 x 5
3 x Bosch^{TM} profile 1	48.9E-3	20 x 20 x 100
3 x L profile 2	0.12	71 x 20 x 8
Aluminium disk 1	0.108	Φ110 x 5
3 x lower spring block	4.5E-3	20 x 15 x 2
3 x M4 threaded rod	28.E-3	Φ4 x 25
3 x Bosch^{TM} profile 2	98.E-3	20 x 20 x 200
Spring support	30.E-3	Φ90 x 12
Aluminium disk 1	34.62E-3	Φ100 x 2
3 x rectangular profile	36.E-3	30 x 20 x 25
3 x Teflon^{TM} guide	32.1E-3	25 x 5 x 60
Aluminium disk 2	0.172	Φ100 x 3
Probe	0.218	Φ50
Spring support	30.E-3	Φ165 x 3
Spacers, screws	99.E-3	-
Total	1.118	Φ263 x 300

Table 3.1: GUN component's masses and dimensions

3.1.1 Spring features

Four different spring has been designed for the GUN system: a spring for ground tests and three springs with different properties for the campaign. The following table (Tab. 3.2) shows the dimensions, the elastic constant and the mass of the springs.

	Microgravity springs			**Gravity spring**
	1^{st}	2^{nd}	3^{rd}	
K [Nm-1]	17	35	83	2530
Dimension [mm]	Φ45 x 70	Φ45 x 70	Φ50 x 90	Φ50 x 70
mass [kg]	5.845E-3	8.415E-3	21.E-3	0.2

Table 3.2: Springs characteristics

3.2 Spring choice and dimensioning

The launch unit operation is very simple: the probe is propelled by a spring that stores energy when it is compressed, and then transmit it to the chaser unit during the microgravity phase. When the spring is decompressed, the entire energy is not transmitted to the probe but part of it is retained by the spring and part of it is lost due to friction. An accurate estimate of the friction was really hard since in microgravity its effects were hard to assess and predict. At first some considerations were made in order to gauge at least its order of magnitude. The energy loss due to friction were considered to be 20% of the total energy stored in the spring.
As told above, the energy of the spring is partially divided in kinetic energy of the spring Ring (the set of aluminium disk 1, aluminium disk 2, Teflon^{TM} guides and the rectangular profiles) and probe and in friction losses, so the spring energy balance is:

$$U_s = \frac{1}{2}K_s x^2 = E_{k,p} + E_{k,s} + E_{k,R} + U_{loss,friction}$$

In the equation, the various terms represents the following physical parameters:

- U_s, potential energy of the spring
- K_s, elastic constant of the spring
- x, spring compression
- $E_{k,p}$, kinetic energy of the probe
- $E_{k,s}$, kinetic energy of the spring
- $E_{k,R}$, kinetic energy of the Ring
- $U_{loss,f}$, work performed by the friction

The kinetic energy of the probe and the Ring is very easy to calculate since the velocity v and the masses m_R, m_p are known.

$$E_{k,p+R} = \frac{1}{2}(m_R + m_p)v^2$$

The kinetic energy of the spring in each part along its vertical axis is different because the spring has one hand fixed to the GUN, while the other can move freely at the velocity of the probe and Ring. Since the velocity of the spring varies from 0 to v it has been assumed a linear velocity grown along the spring length; for a generic infinitesimal spring part the kinetic energy is:

$$dE_{k,s} = \frac{1}{2}dmv(x)^2 = 0.5\rho dx(\frac{x}{l}v)^2$$

Integrating in the length of the spring the following expression is obtained:

$$E_{k,s} = \frac{1}{6}m_s v^2$$

The complete formulation previously reported can be written as:

$$\frac{1}{2}K_s x^2 = \frac{1}{2}(m_R + m_p + \frac{1}{3}m_s)v^2 + U_{loss,f}$$

In this expression, once the energy loss component of the friction $U_{loss,f}$ was determined, the only unknown component was the x compression variable of the spring. The friction work was not easy to determine since it didn't only depend on the sliding friction coefficient of the materials (aluminium and Teflon^{TM}), but also on the contact area and transmission angle of the force with respect to the vertical direction.
The first calculation for the spring compression has been conducted on a gravity spring, and then a complete friction analysis has been made. Since FELDs needed to be operative in gravity conditions, for the laboratory tests in Padua a gravity spring has been used (Fig. 3.12).

For the gravity spring the gravitational potential energy has been considered. In ground condition the velocity v is not the velocity estimated with the probe dynamic analysis for microgravity conditions, but a velocity v_1 that can allow the probe to reach the SEC with the required v velocity. The expression of the velocity v_1 is:

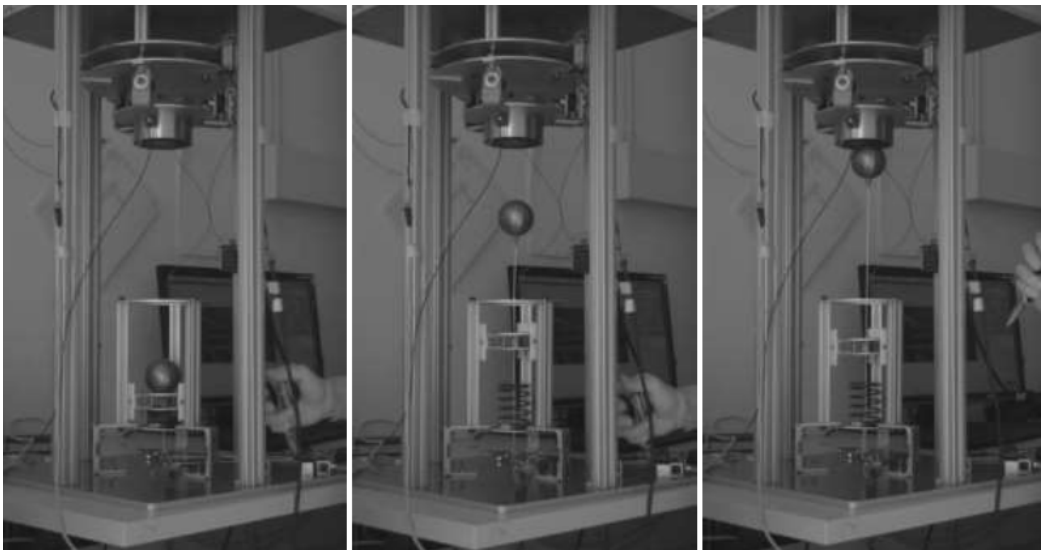

Fig. 3.12: Ground test of FELDs Experiment at CISAS laboratory

$$v_1 = v + 2gh$$

Due to gravity, the spring and the ring gain potential energy during the spring decompression and probe rising; the expression of their potential energy is:

$$U_1 = (m_R + m_p)gx$$

Considering the spring density to be linear in length, the potential gravity energy of the spring can be written as:

$$U_{s,g} = m_s g \frac{x}{2}$$

The energy balance still depends on the friction work and can be rewritten as:

$$\frac{1}{2}K_s x^2 = 0.5(m_R + m_p + \frac{m_s}{3})v_1^2 + U_{l,f} + (m_R + m_p + \frac{m_s}{2})gx$$

3.2.1 Friction losses

In microgravity environment friction forces are lower by order of magnitude than friction forces in ground conditions. To firstly estimate the friction losses, it has been considered the worst-case scenario, assuming that in the worst case, microgravity friction could be equal to gravity friction.
The friction force between two surfaces is directly proportional to the normal component of the force that presses them together. The only relevant contact force that could cause friction is the force that the ring exerts on the guide during the decompression of the spring. Since the only situation in which the worst case could present itself is when the ring is larger than the guides, the ring has been designed slightly narrower than the guides, leaving a play of 0.2 mm between the two surfaces. The play between the Teflon^{TM} guide and the Bosch^{TM} profile allowed to exclude the worst case, which has been considered as a safety margin in the spring compression calculations. As previously told, the only contact force acting on the surfaces during the decompression phase is the elastic forces of the spring, so the friction has been gauged as:

$$F_f = kx \sin(\theta)\mu$$

θ represents the angle between the vertical axis (theoretical decompression direction) and the real decompression direction.
At this point the other last term to value was the dynamic friction coefficient μ. The static friction coefficient has been determined simply gradually tilting the GUN and finding the smallest angle at which the ring started to slide on the guides:

$$\mu_s = \tan(\theta)$$

The angle found was 8.5° leading to a static friction coefficient of $\mu_s = 0.15$.
Another method to determine the friction consisted in sliding the Ring upward with a wire running through a pulley placed directly above the GUN. The pulley ensured that the Ring's movement was as vertical as possible, limiting the friction to a point that as been assumed similar to the microgravity value (Fig. 3.13).

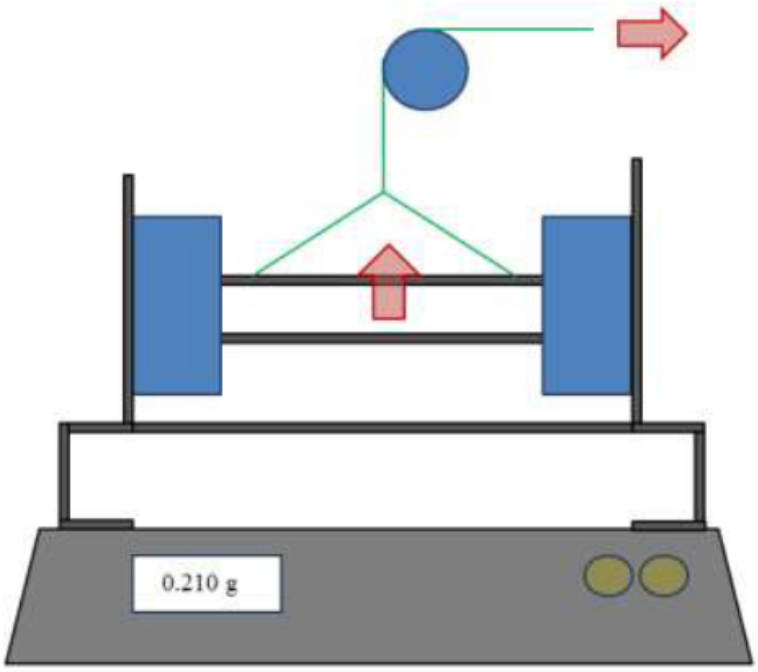

Fig. 3.13: Pulley system to measure friction

Under the GUN a precision scale was placed to measure the weight force of the structure. The scale had the role to measure the difference of weight due to friction's action: when the Ring slid upwards the friction pushed the ring downwards and the GUN structure upwards, so the scale measured a lower weight. The difference between the weights measured was taken as the friction value. This system allowed to determine, with a precision of 10^{-3} kg, a range of values of friction going from 0.02 N to 0.1 N. For safety reasons the highest value of 0.1 N has been assumed as the friction during the entire decompression phase. With the energy balance for the micro-gravity spring and posing the friction work to be $U_{l,f} = 0.1N * x$ it was possible to determine the spring's compression x that gave the required velocity v by iteration.

$$\frac{1}{2}K_s x^2 = \frac{1}{2}(m_R + m_p + \frac{m_s}{3})v^2 + F_f x$$

The results obtained with this balance are very closed to the energy loss estimated for the design process of the launch unit: the three microgravity

springs designed showed a percentage of friction loss energy around 20% in their compression range.

3.2.2 Spring dimensioning

To design the spring of the launch unit, the most important parameter was its elastic constant K.
For the microgravity tests, three different springs have been considered:

- 1^{st} spring, elastic constant of 17 Nm-1
- 2^{nd} spring, elastic constant of 35 Nm-1
- 3^{rd} spring, elastic constant of 83 Nm-1

During the gravity tests in Padua a gravity spring with an elastic of 2530 Nm-1 has been used.
The elastic constant of each springs has been calculated with the following formula:

$$K = \frac{Gd^4}{64i(\frac{D}{2})^3}$$

The characteristics of the microgravity springs are shown in Tab. 3.3.

d [mm]	**L_0 [mm]**	**L_{min} [mm]**	**D_{ext} [mm]**	**K [Nm^{-1}]**	**m [kg]**	**i**
1.25	70	25	45	17	5.845E-3	6.5
1.25	70	25	45	35	8.145E-3	6.5
1.6	90	25	50	83	21.E-3	6.5

Table 3.3: Characteristics of the microgravity springs

The parameters in Tab. 3.3 are:

- d, diameter of the wire
- L_0, resting length
- L_{min}, length at maximum load

- D_{ext}, spring external diameter
- K, spring elastic constant
- G, material constant
- i, useful number of usable spring turns
- D, medium diameter of the spring
- m, mass of the spring

The springs were composed of steel with a density of $\rho = 8300$ kgm-3 and the expression of their volume is given by the spring thickness $\pi(\frac{d}{2})^2$ and length $(i + 1.5)\pi D_m$, where i is the number of useful spires.
The mass of the springs can be obtained as:

$$m_s = \rho\pi(\frac{d}{2})^2(i + 1.5)\pi D_m$$

The L_{min} (length at maximum load) should be intended as the maximum spring compression that does not compromise its integrity.
The results showed that commercially available springs were enough for the needed requirements, while custom springs with higher thickness would have had a high elastic constant, with all the precision issued this entails. An excellent elastic constant, assuming that it remained in linear regime for the whole compression, was around a hundred Nm-1, with a suitable diameter of 1.25 mm, or 1.6 mm. For this reason during the test campaign only the third spring, with an elastic constant of $K = 83$ Nm-1 has been employed.
This spring made it possible to give the probe the required kinetic energy even in the worst case presented earlier.

The following graph (Fig. 3.14) summarizes the safety margin given by the 83 Nm-1.

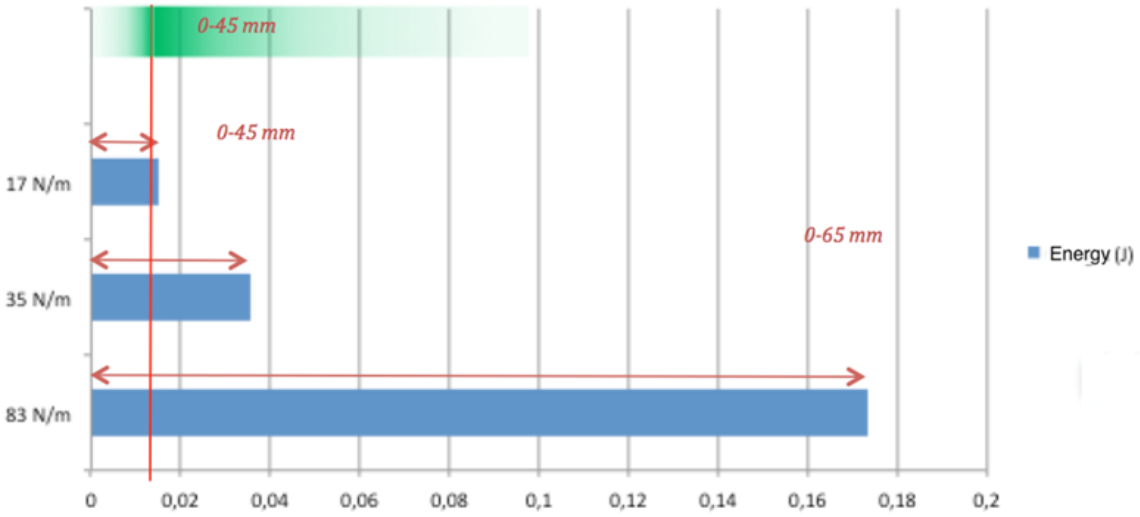

Fig. 3.14: Spring energy diagram

The x axis represents the compression energy and the vertical red line indicates the required compression energy to eject the probe towards the SEC with the desired initial velocity.
The green colour represents the probability of needing a given compression. All the calculations, the empirical empirical tests, and the successful drops, confirmed an energy loss of about 20% of the initial value.

3.3 Structural load simulation

One of the key aspect of the design process of the launch subsystem was to conceive a structure which could both allow to have an almost impulsive shot with minimal friction losses and support the heavy loads due to the capsule landing in the deceleration chamber. As for the SEC subsystem, a finite-element analysis was performed with ANSYS, considering the worst-case load (50g deceleration during the impact of the capsule with the ground) in the critical component of this unit (its support). After the analysis, to make sure that the GUN structure does not suffer any damages during the capsule impact with the ground, the aluminium bar connected to the L profile in the figure as been replaced with a 20 mm x 20 mm x 100 mm Bosch™ profile. Since even the bar showed stresses under the material yielding point the configuration with the bar as been taken as backup solution. As for the SEC subsystem, two types of analysis were conducted: a linear static one, and a non linear static one, to verify if there was some cause of non linearity in the model. The results obtained in the two analyzes were identical, therefore only the ones referring to the linear one are reported (Fig. 3.15).

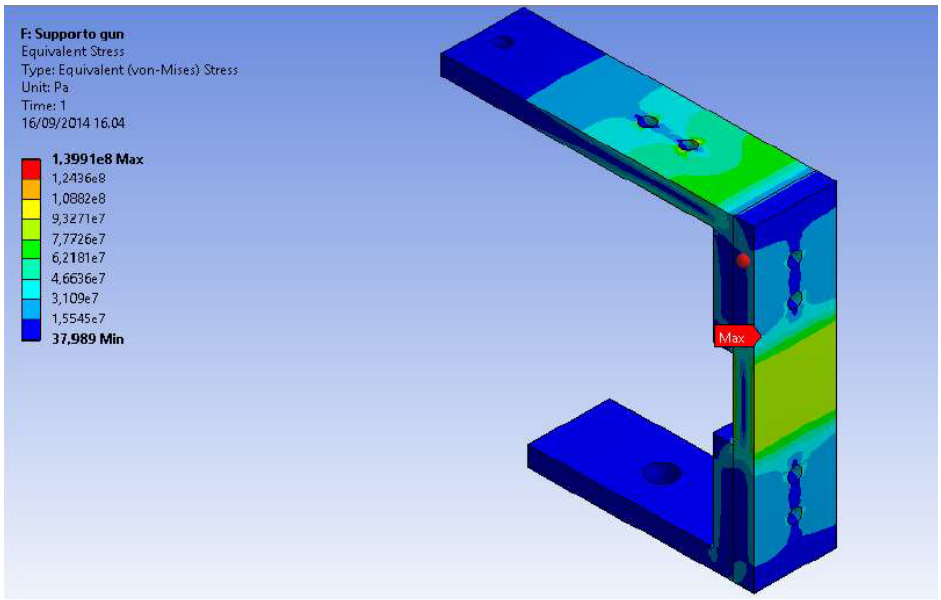

Fig. 3.15: Load on GUN support

After analyzing the results related to the finite element analysis the 6082 aluminium alloy was selected to realize the various components of the system, as its yield stress leaves an ample safety margins over the expected equivalent stresses.

Chapter 4

Results

Docking maneuver required forces as small as possible on the target system. As mentioned in chapter 2, the SEC system has been conceived and designed with the aim of testing a dampened system able to attenuate the dynamic load of the impact and to eliminate the response oscillations in the shortest time possible. The SEC however, is provided with load cells that measured its dynamic response; for this reason the design process required a particular attention as it was not enough to conceive a simple dampened system. This subsystem also had to be integrated in the ZARM Drop Capsule so as to be able to change all its components with relative ease in case of failure, or to vary its stiffness and damping properties in relation to the needs of the test campaign. Finally, since the system was integrated in the capsule above the GUN, it had to be provided with a security system to prevent the entire hardware from falling on the GUN during the capsule's impact with the ground at the end of the falling phase. In order to choose the load cells and to predict the timing of damping of the system, the SEC has been modeled as two oscillating masses with damping and stiffness parameters defined as in chapter 2. The response of the simulation has allowed to predict with an acceptable accuracy the true response of this subsystem. Unluckily, only the first three Drops had been successful: the following two tables shows the conditions of the SEC and GUN for the five microgravity tests (Tab 4.1 - Tab 4.2).

Parameters	1^{st} **Drop**	2^{nd} **Drop**	3^{rd} **Drop**
Spring's compression $[mm]$	21	12	12
Probe's velocity $[\frac{m}{s}]$	0.23	0.14	0.14
GUN-SEC distance $[mm]$	340	340	340
GUN-SEC positioning	aligned	aligned	aligned

Table 4.1: Experiment conditions, first three Drops

Parameters	4^{th} **Drop**	5^{th} **Drop**
Spring's compression $[mm]$	12	12
Probe's velocity $[\frac{m}{s}]$	0.14	0.14
GUN-SEC distance $[mm]$	340	410
GUN-SEC misalignment	2.5°	2.5°

Table 4.2: Experiment conditions, last two Drops

For manufacturing errors, the first three Drops was characterized by a misalignment in the probe trajectory. For this reason in the last two Drops the GUN has been misaligned by 2.5° by adding some nuts on its supports, thus correcting the manufacturing error in order to obtain a precise vertical and aligned trajectory of the probe between SEC and GUN. In the 4^{th} Drop, the docking was not successful, as the tether got stuck to the screw positioned in the middle of the GUN and, due to the friction between the tether and the screw, the probe didn't reach the electromagnet and fell down during the capsule deceleration. The camera next to the Release system helped to understand how the tether got stuck: as soon as the constantan started to burn, the energy of the torsion spring sent the tether directly to the middle screw, making it bunch up between the screw and the plexiglass™ tube and increasing its friction. Looking at the torsion spring energy, in the 5^{th} Drop the spring was removed in order to have less energy and unwind the tether more slowly. As an alternative to the spring, a ring of a thinner wire between the constantan and the tether was used. The idea was to reduce the energy and eliminate the risk of bunching the tether up in the center of the GUN. In the final Drop, the docking wasn't obtained because of additional complications with the release system. Despite replacing the spring with the ring, the tether got stuck between the plexiglass™ tube and the middle

screw.

4.1 Load cells data analysis

The load cells were used to measure the forces exerted on the SEC subsystem when the probe impacted on the electromagnet, as well as getting an understanding of the force exerted on the probe by the electromagnet itself. The load cell data were necessary to study the dynamic response of the SEC, both in the time and frequency domains; the influence of the various events during the experiment (the capsule release, the probe impact and the capsule deceleration) had clear effects on the sensors. The measurements were collected with three load cells positioned as in (Fig. 4.1)

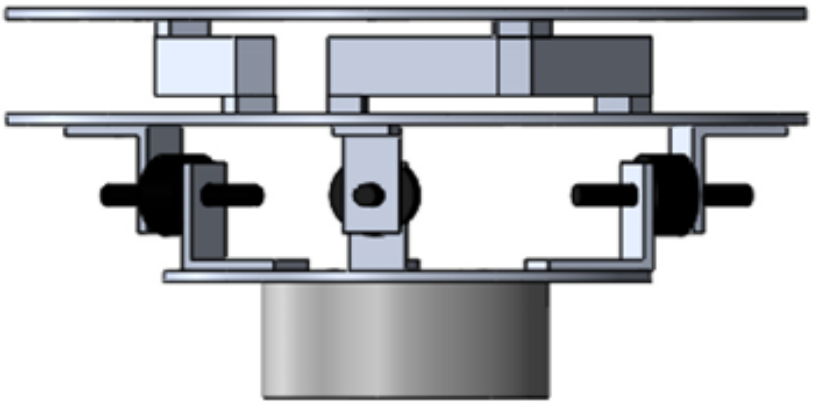

Fig. 4.1: Load cells position on the SEC

This positioning allowed to gauge the spatial position on which the forces acted, as well as ensuring the structural stability of the system. As already explained, the load cell output was connected to a signal amplifier, with a distance from the cells and the amplifier reduced to minimum to minimize the thermal noise in cables, power dispersion and other electromagnetic disturbances. The amplifiers expected a 2 $\frac{mV}{V}$ sensitivity and have a maximum output voltage of $\pm$ 10 V on a linear scale, with an uncertainty within 10 ppm. The linearity of the amplification was guaranteed by the fact that the -3 dB bandwidth was 30 kHz, while the simulations showed that the expected

response was 3 decades lower. The output of the amplifier was registered and saved by the CSS, which used a 16 bit ADC to digitalise the analog signal; a quantization range of $\pm 10V$ was set via software in order to fully exploit the quantizer and lower the quantization error; the uncertainty introduced by the ADC was about $2 * 10^{-5}$. Shielded cables were used to connect the amplifiers with the CSS, so as to reduce external noise. The uncertainty on the measurements (which were performed with the electromagnet turned on so as to avoid the EM effects when it was activated) was mostly due to the load cells; considering possible unspecified SNR problems at the amplifier, and that the shielded cables were around 40 cm long, a security factor of one order of magnitude was used. A data up to the second decimal point was exploited, with a relative uncertainty of 10^{-3}; the measurements had a 3g step, with maximum values of $\pm 3kg$. The sampling frequency was 4950 samples/s for the first drop and 1000 samples/s for the other four, high enough to detect the expected dynamic response without bias and perform the relevant analyses in the frequency domain. Another important factor was the load cell mounting: the balancing to obtain correct data required great attention. Before the first drop, the load cells were laid on a plane, so that they were on their resting point and their output was 0; the amplifiers were then tuned to minimize the offset, and the cells were then disconnected and mounted on the SEC. After mounting the whole setup on the upper platform, the cells were connected to the amplifiers and balanced by mechanically adjusting the screws so that all cells had the same output. Once the system was balanced, the measurement system was verified with different loads. In later drops, some difficulties were experienced because of the force of the final impact; this prevented a fine mechanical balancing, and the balancing was done in post-processing with appropriate offsets and correcting factors. The measured data was available live via a LabView VI: the information the load cells gave the CSS were saved in a plaintext file. The first analysis was performed directly on the control room computer with a National Instruments proprietary tool, and they were useful to understand the sequence of events in the experiment and consider the possible changes for the subsequent drops. Most of the actual analysis was performed in Matlab after retrieving the data

from the capsule. The processing aimed at deriving both the behavior in the time domain and the frequency response of the SEC.
Subsections 4.1.1 - 4.1.2 - 4.1.3 report respectively the plots of the force temporal evolution and the plots of the frequency domain of the first, second and third Drop; since the graphs obtained in the three tests are very similar, the results are described in section 4.2. The force temporal evolution of each Drop shows the phases of the experiment: the capsule begins its free fall after about 2 seconds, then the probe hits the SEC at the 4.3 second mark; finally, the capsule hits the deceleration chamber after 6.7 seconds, maxing the load cell output.
The plots of the analysis in the frequency domain consider the period between 2 and 3.5 seconds, and after a Fast Fourier Transform (FFT) the results have a frequency granularity of 0.7 Hz, enough to detect two peaks (at 24 and 30 Hz) with a rectangular window.

4.1.1 First Drop

For the 1^{st} Drop the experiment has been prepared in the nominal situation of the simulation. The characteristics of the nominal configuration are:

- aligned SEC and GUN, relative distance of 340 mm
- spring compression of 21 mm in order to obtain a mean probe velocity of 0.23 ms-1
- no cap

The 1^{st} Drop was successful: after 2.5 s the probe bumped against the electromagnet twice and then successfully docked.
Due to manufacturing problems of the components, the probe didn't reach the electromagnet perfectly straight (the probe was about 2.5° off from the electromagnet's center).
The following figures (Fig. 4.2 - Fig. 4.3) shows the frequency response of the SEC and the output of the load cells obtained.

The release system worked without getting stuck, as the tether rewinding was clear and almost frictionless.

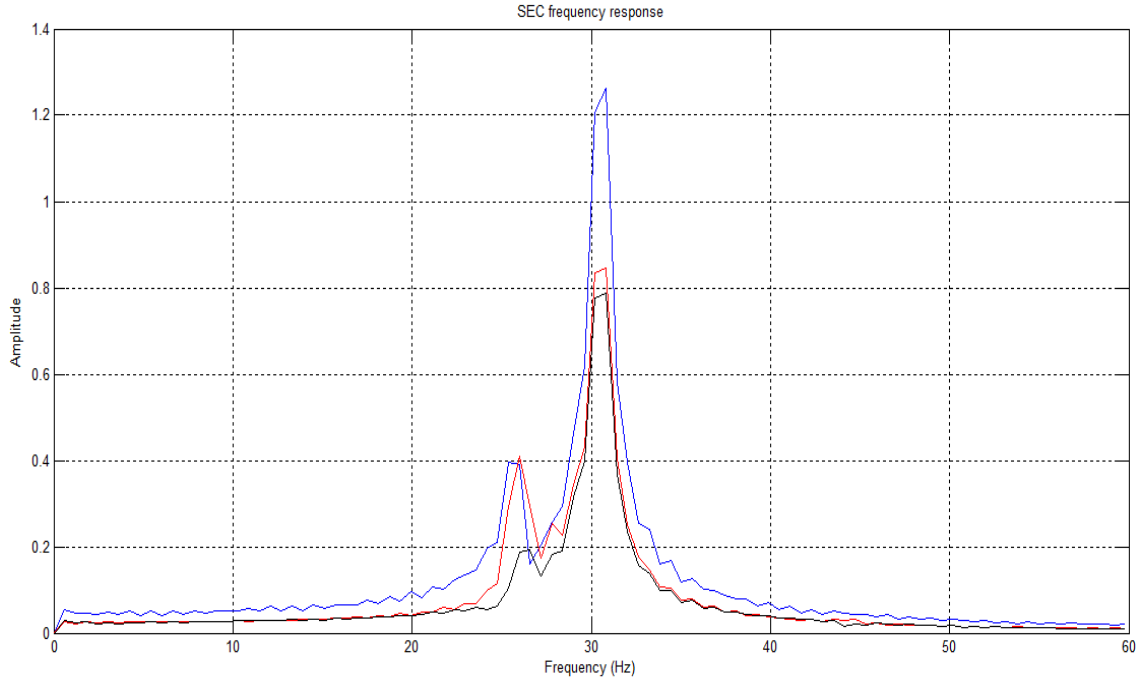

Fig. 4.2: SEC frequency response, 1^{st} Drop

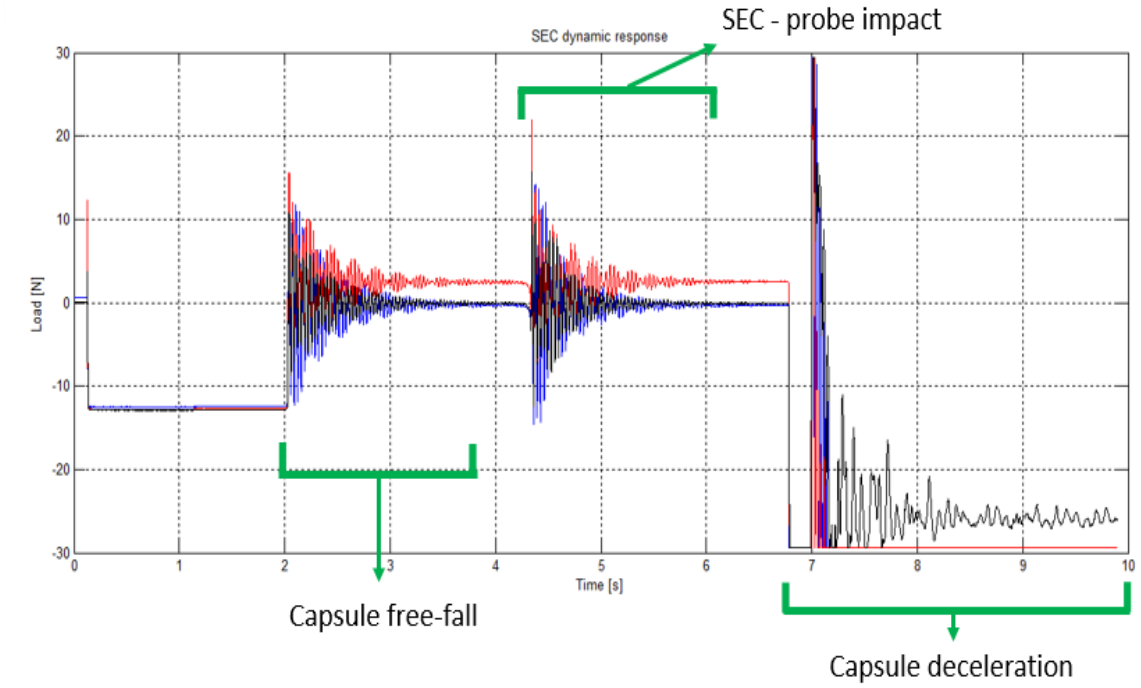

Fig. 4.3: Dynamic response of the SEC, 1^{st} Drop

4.1.2 Second Drop

Analysing the videos, it has been noted that the probe velocity in proximity of the electromagnet was too high; after the first contact with the electromagnet, the probe bumped two times before docking. For this reason, the probe velocity has been reduced from 0.23 ms-1 to 0.14 ms-1, compressing the spring by 12 mm. The experiment parameters for the 2^{nd} Drop were:

- aligned SEC and GUN, relative distance of 340 mm
- spring compression of 12 mm in order to obtain a mean probe velocity of 0.14 ms-1
- no cap

The 2^{nd} Drop was also successful: the Probe arrived to the electromagnet more slowly and it was possible to see the capture effect of the electromagnet and its sphere of influence. The same misalignment observed in the first drop presented itself again; the release system also worked like in the 1^{st} Drop. The following figures(Fig. 4.4 - Fig. 4.5)shows the frequency response of the SEC and the output of the load cells obtained.

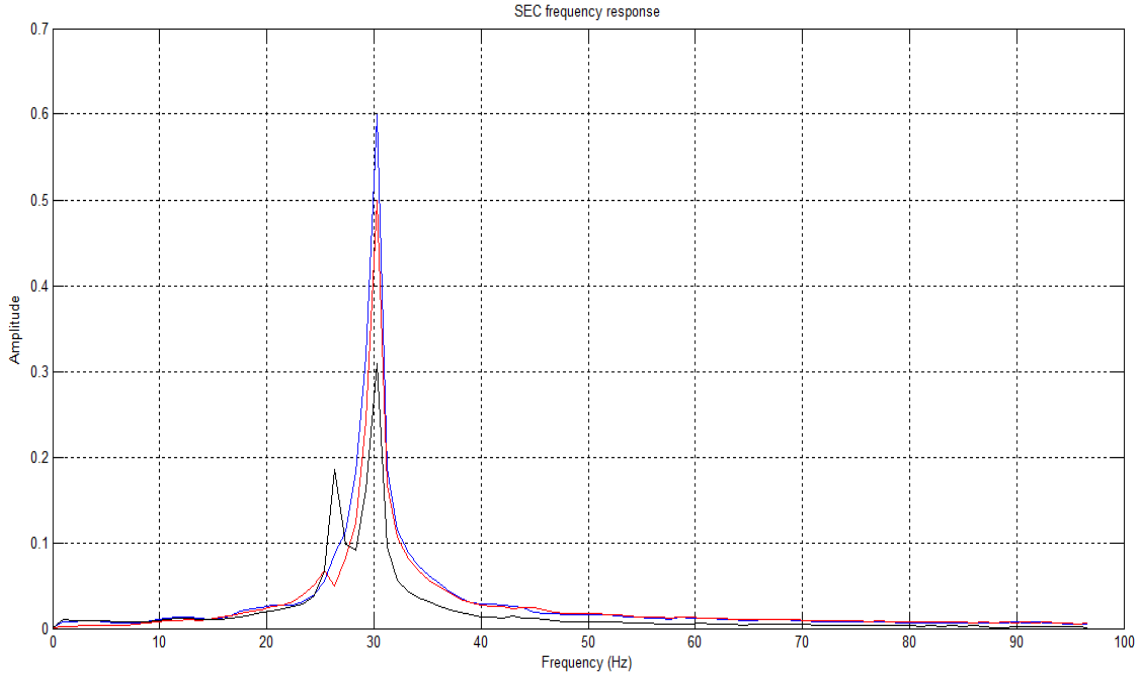

Fig. 4.4: SEC frequency response, 2^{nd} Drop

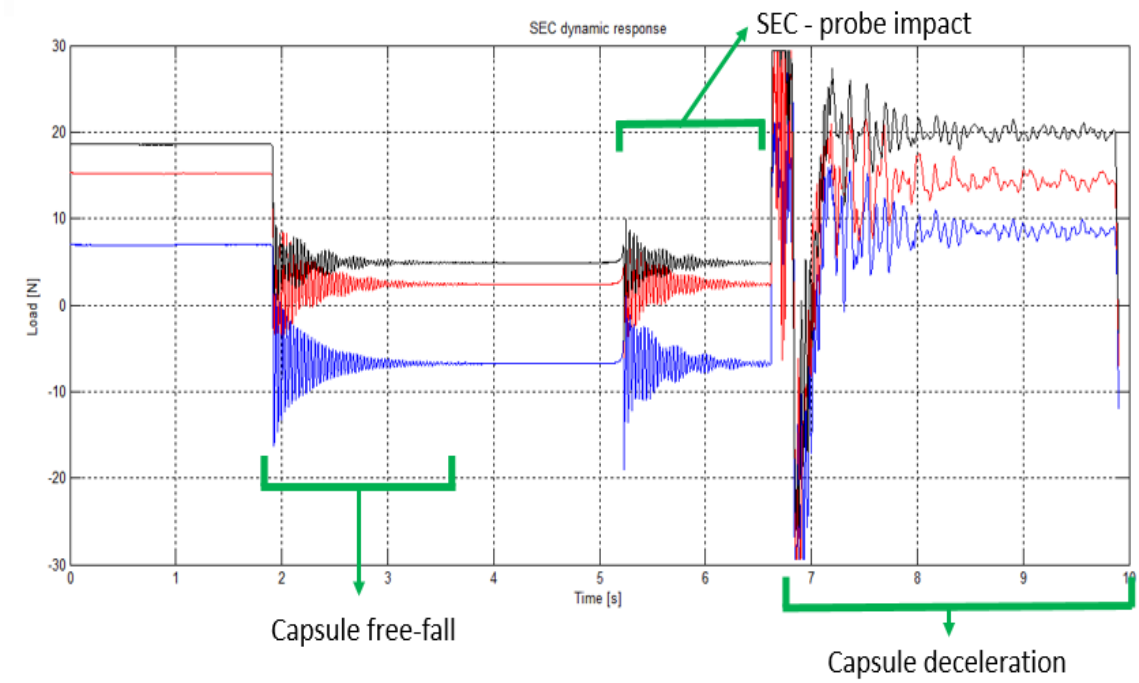

Fig. 4.5: Dynamic response of the SEC, 2^{nd} Drop

4.1.3 Third Drop

Since the data obtained in the 2^{nd} Drop were very good the same parameters were manteined for the 3^{rd} Drop for repeatability:

- aligned SEC and GUN, relative distance of 340 mm
- spring compression of 12 mm in order to obtain a mean probe velocity of 0.14 ms-1
- no cap

The following figures (Fig. 4.6 - Fig. 4.7) shows the frequency response of the SEC and the output of the load cells obtained.

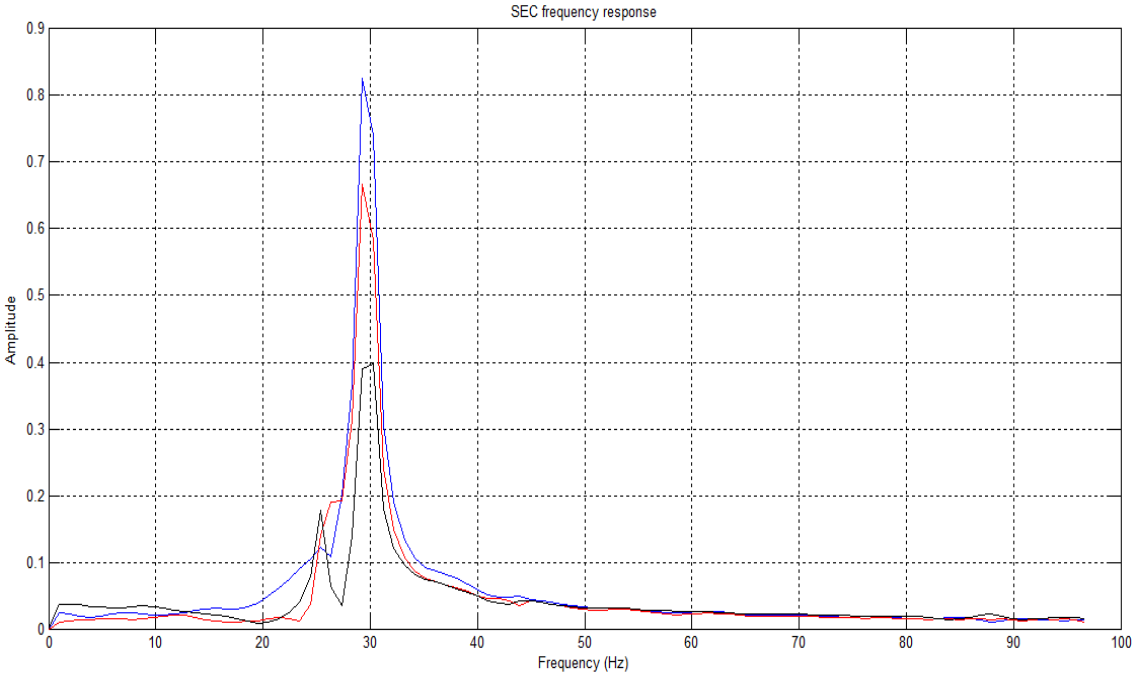

Fig. 4.6: SEC frequency response, 3^{rd} Drop

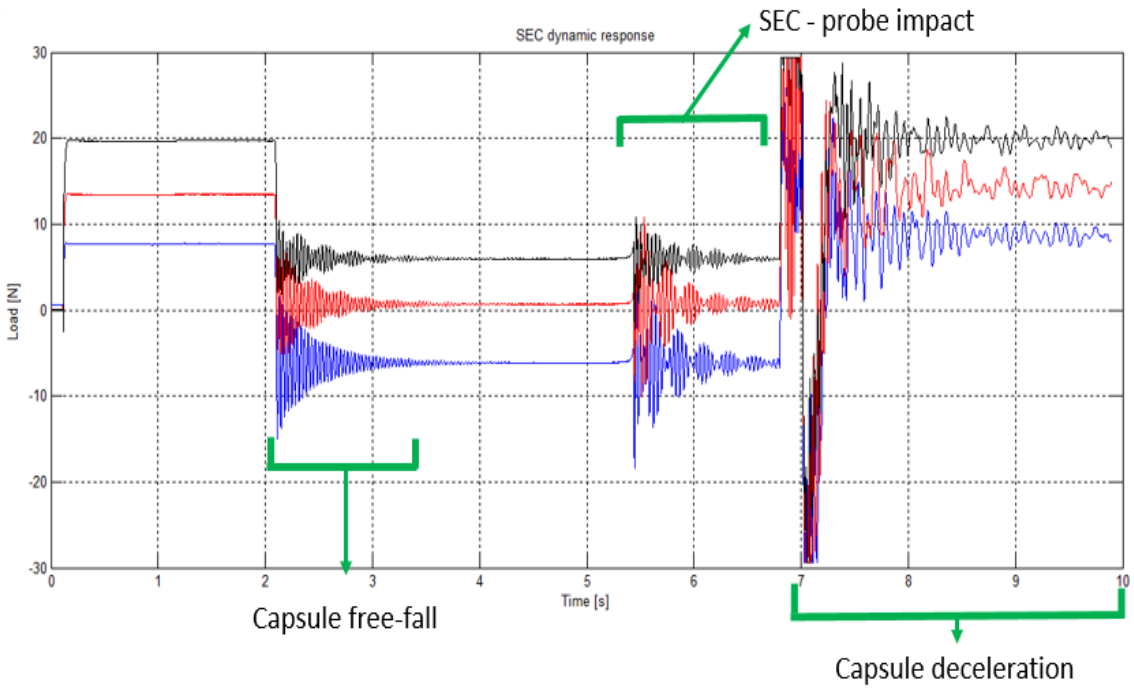

Fig. 4.7: Dynamic response of the SEC, 3^{rd} Drop

The 3^{rd} Drop was successful; as expected, the results were very similar to the 2^{nd} Drop. Both the probe trajectory and the magnetic capture effect were very similar to the previous ones. As in the 1^{st} and the 2^{nd} Drop, there was a misalignment in the probe trajectory.

4.2 Theoretical vs real trends

The graph in figure Fig. 4.8 compares the trend obtained with the simulation, using the parameters of elasticity and damping that had been taken from the data-sheet (red line) and the trend of a real load cell obtained during the 3^{rd} Drop.

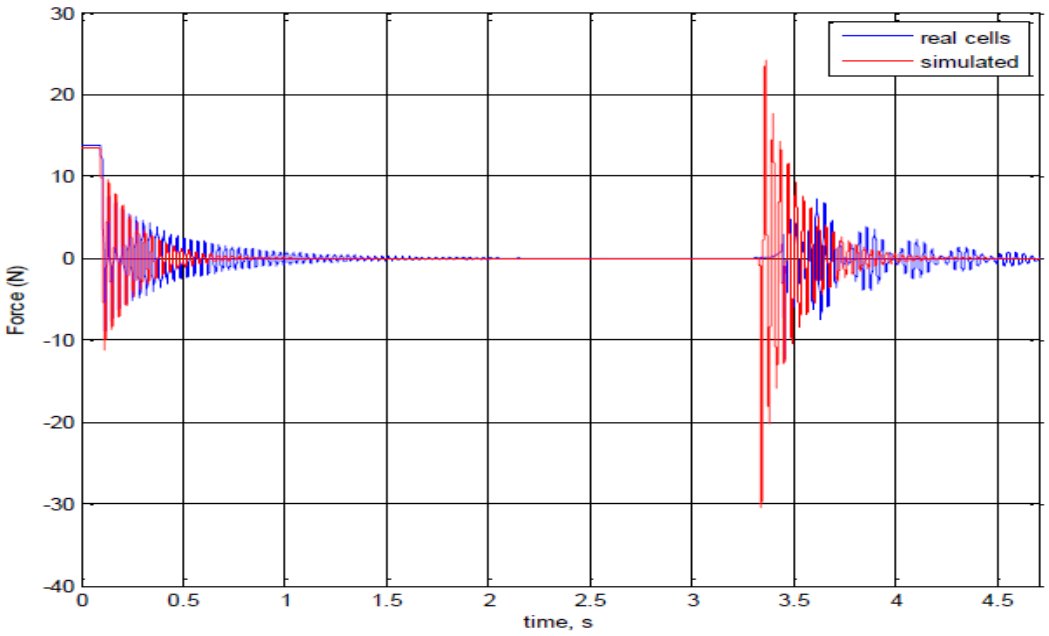

Fig. 4.8: Dynamic response of the SEC obtained by the simulations

As the plot shows, due to the great simplifications that were made in the theoretical model, the damping time of the response and the amplitude of the oscillation does not match between simulation and real case. It was also not expected a second oscillation of the system (secondary), which caused a beat in response to impact of each individual load cell. Since the beat did not show in the simulation, looking at the plot some considerations about the nature of this phenomenon have been made, and the reason for this development has been hypothesised.
The first reason to explain the phenomenon is that the damping effect of the

load cells in the simulation is negligible compared to the damping effect of the dampers. If the two damping effects were comparable, each of the two masses (electromagnet and structure) would continue its oscillatory motion about the same time and the motion of any one of the two masses would thus be influenced by the motion of the other. This explanation is not reflected in the real case because the frequency that causes the beat in the real case only varies the amplitude, without changing the basic position. The following figure (Fig. 4.9) shows a simplified system that highlight this phenomenon.

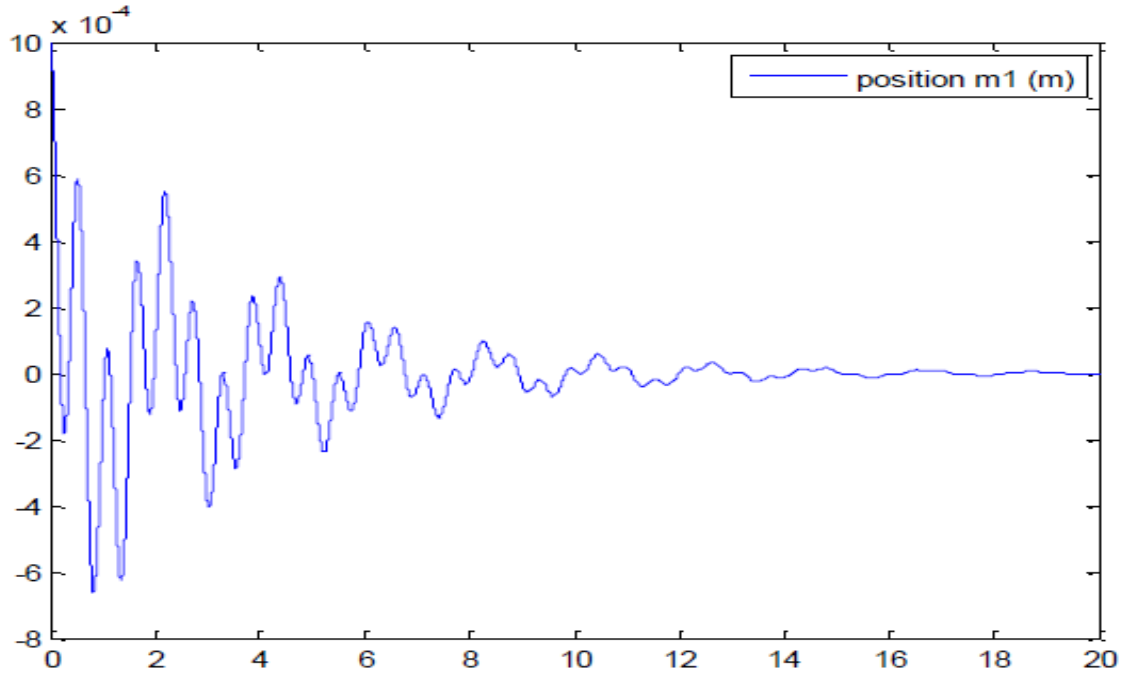

Fig. 4.9: Damping effect of the cells

It is evident that the second resonant frequency must be due to a movement of the SEC in a non-axial direction (Fig. 4.10). The prove of that can be found looking at the real response after the impact: the beats are stronger after the impact with the probe and this is probably due to the impact position. An impact outside the center of the electromagnet may have rotated the SEC and cause the unexpected response. The weaker beats that have occurred from the beginning of the free fall phase to the instant before the impact may be due to imperfection in the assembly.

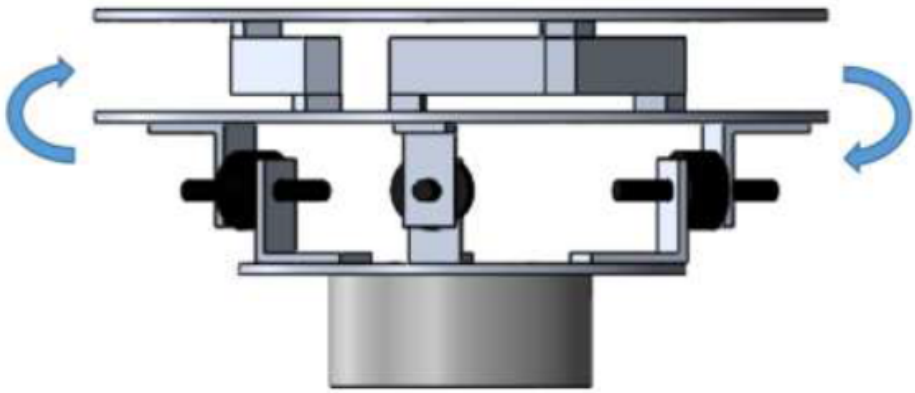

Fig. 4.10: SEC orthogonal rotation

Many other factors can be drawn from the charts and validate this hypothesis than the other. First of all the fact that there has occurred especially after the impact between the probe and the electromagnet, which must have occurred not perfectly central, as can be seen also from the analysis of the position of the probe during the ascent. The sudden absence of gravity only in some cases gave rise to this phenomenon, this is probably due to a non-homogeneous assembly. If fact, some parts of the system in severity were mounted in tension compared to slightly darkened (especially in the second and third Drop), the discharge of the gravity could have enabled the establishment of a non-axial motion. The second fact that supports the hypothesis of the rotation of the SEC is the same frequency of oscillation. Looking for example at the frequency response of the SEC in the first Drop, another relevant fact can be drawn from the graphs and validate this hypothesis (Fig. 4.11).

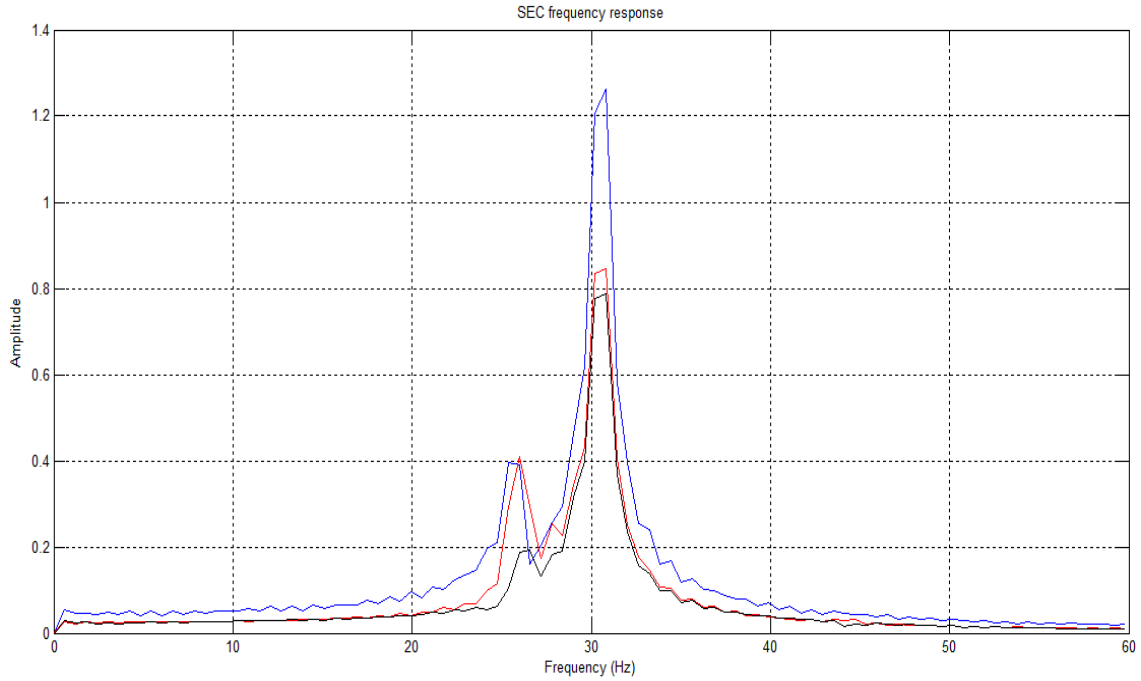

Fig. 4.11: SEC frequency response, 1^{st} Drop

The frequency that has generated the beats was very similar to the main oscillation frequency. This is because the system present a ratio of torsional stiffness combined with that of the cells and the flexural moment of inertia of the structure is very similar to the relationship between the flexural rigidity and the inertial mass of the same. For this reason the SEC presents two phenomena linked by two close oscillation frequencies, leading to a trend similar to the one obtained in the real case. Finally, the secondary frequency, for different cells in the same drop, is out of phase between one cell and the other, as if the movement characterized by this frequency influenced the cells at different times interacting constructively for a cell and destructively for the other (in terms of amplitude) in the same instant, and vice versa in the next instant. This fact seems to be the key to assert that the rotation happened as the figure shows, and that at the same time raising the structure by compressing a cell (constructive interference) lowers the other side stretching the cell on the other side (destructive interference).

4.3 Data obtained

The probe ascent phase and its approach to the electromagnet was visualized with the high velocity cameras and the GoPros. With the use of the cameras, it was possible to see and analyze the position of the probe in every instant and consequently obtain its velocity and acceleration by deriving the position vector in relation to time. The velocities graphs show that the velocity of the probe in proximity of the electromagnet was:

- 0.57 ms-1 in the 1^{st} Drop
- 0.49 ms-1 in the 2^{nd} Drop
- 0.62 ms-1 in the 3^{rd} Drop

To determine the impact energy dissipated by the SEC orthogonal rotation, by the deformation of the probe and the electromagnet and by other eventual cause of dissipation, a further study has been conducted. During the impact the kinetic energy of the probe is partially converted in potential energy and partially dissipated as:

$$\frac{1}{2}m_s v_s^2 = \frac{1}{2}K_{cells}\Delta x^2 + U_{diss}$$

In the above formula the parameters are:

- $U_{k,system} = \frac{1}{2}K_{cells}\Delta x^2$, potential energy absorbed by the SEC in axial direction
- $\frac{1}{2}m_s v_s^2$ kinetic energy of the probe at the impact with the SEC
- U_{diss}, dissipated energy

The SEC had a total mass of 4.92 kg and its potential energy can be calculated relatively easily considering the stiffness of the load cells. A quantitative measure of how the system disperse energy can be obtained by the dampers' action.
The damping time observed from the load cells data is almost the same in all the drops and is equal to 1.6 second. During this time, the absorbed potential energy can be expressed as:

$$U_{k,system} = \frac{1}{2} K_{cells} \Delta x^2$$

Considering a stiffness of the load cells of approximately 75000 Nm-1 and a displacement under the weight of the structure of 0.18 mm, calculated observing the load cell warping (45% of their maximum warping) in the Drop test, the absorbed potential energy in the axial direction is approximately 3.8E-3 J. The collision of the probe, (which has a mass of 0.218 kg), with the SEC is absorbed in almost the same time with a slightly higher amplitude than after the gravity release.
The simulations also proved that most of the probe's kinetic energy came from the electromagnetic attraction, with only a small part coming from the GUN shot.
From the energy balance is possible to have an estimate of the percentages of the dissipated energy:

- 90.3%, 1^{st} Drop
- 84.6%, 2^{nd} Drop
- 90.5%, 3^{rd} Drop

The values of the dissipated energy are relatively high since they depends to several causes: the electromagnet and sphere material deformation, the friction due to the probe's relative motion on the electromagnet surface and the non-axial motion of the SEC system.

The test campaign confirmed the effectiveness of a damped system for the capture of a lightweight interface approach, given the reduced damping time even though the inertia of the receiving system was relatively high.
Reducing the mass of the components even further may increase the damping capability of the technology for space application.
During the test campaign it was not possible to measure the high-frequency disturbances due to the load cell sampling frequency, but the dampers should have absorbed any high-frequency vibrations.
Even if the simulation did not match the experimental results exactly, it allowed a good prediction of the damping times and a good choice of load cells

for the reading of the system's response. Due to many uncertain factors in the calculations, it was not possible to accurately measure the magnetic force from the load cell readings; however a qualitative estimate of the magnetic force can be seen in the following figure (Fig. 4.12).

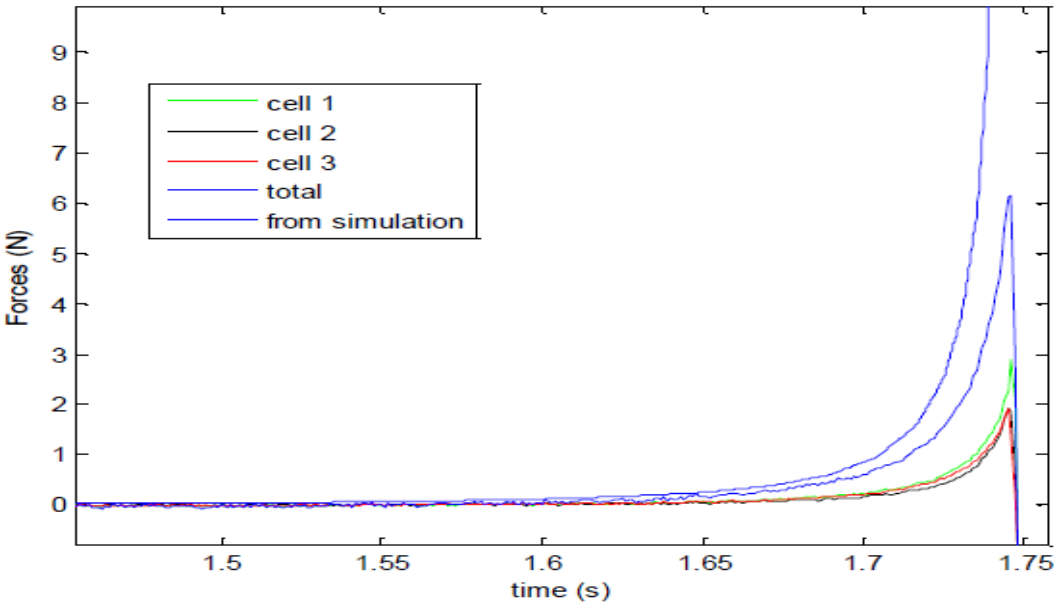

Fig. 4.12: Load cells forces, real and simulated trends

This reading may not be reflected in the simulations, as they are based on interpolation of values of the forces derived ideally with a simulator, and then resized to match the true performance with the simulated one. In addition, the inertia of the SEC itself, along with the action of the dampers, prevents a correct reading of the forces.

Chapter 5

Conclusion

This thesis described the mechanical design and development of a novel soft docking concept that explained the performance of an innovative tethered soft docking system whose main objective was to guarantee a post-docking mechanical connection through the use of a flexible wire and proved its effectiveness through simulation and experimental results. The experiment was a successful proof of concept for the FELDs technology. The three successful dockings proved the capture effect of the magnetic field and the possible benefits of a tethered docking system. The drops validated the model of the SEC response to the impact, as well as providing important data on the behaviour of the probe and the magnetic field. The analysis of the mechanical behaviour of the SEC in low gravity showed that a damped system like FELDs is suitable to implement the target interface of a docking system: the effectiveness of the damped system to capture a light weight probe was confirmed by the very short damping time.
The data collected by the load cells showed that a damped receiving interface is viable for small satellites, as it validates the the model of the SEC response.
A target interface as the SEC system is capable to dampen and absorb the energy of the impact between the probe and the magnetic receiving interface lowering to minimum the disturbances on the target spacecraft.
FELDs could enlarge the state of the art of docking technology for small

satellites, which is already a completely unexplored field: the experiment success is the first step towards a full space-viable implementation of the system. Although the results were very encouraging, there still are some issues to work on: the tether release system needs to be perfected to be more reliable, and future experiments would benefit from higher precision in the system construction and sensors. These drops provided proof that the concept is valid, and developing it further to make it more efficient and reliable should be the next step.

Bibliography

[1] Hinman, Elaine M., and David M. Bushman. "Soviet automated rendezvous and docking system overview." *Automated Rendezvous and Capture Review. Executive Summary.* Vol. 1. 1991.

[2] Miller, D., Saenz-Otero, A., Wertz, J., Chen, A., Berkowski, G., Brodel,. "SPHERES: a tested for long duration satellite formation flying in microgravity conditions." *In Proceedings of the AAS/AIAA Space Flight Mechanics Meeting*, Clearwater, FL, Paper No. AAS 00-110.

[3] Pavlich, J. C., Tchoryk Jr, P., Hays, A. B., Wassick, G. "KC-135 zero-G testing of a microsatellite docking mechanism." *In Aero Sense 2003 (pp. 31-42).*, International Society for Optics and Photonics.

[4] Boesso, A., and A. Francesconi. "ARCADE small-scale docking mechanism for micro-satellites." *Acta Astronautica* 86 (2013): 77-87.

[5] Lewis, James L., et al. "Advanced Docking System With Magnetic Initial Capture." (2004).

[6] Olivieri, L., Antonello, A., Savioli, L., Francesconi, A., Dynamic behavior of a Semi-Androgynous small satellite docking interface. *65th IAC, Toronto, Canada*, 29 September – 03 October 2014

[7] Dittus, Hansjörg. "Drop tower 'Bremen': a weightlessness laboratory on Earth." *Endeavour* 15.2 (1991): 72-78.

[8] "http://www.newtonmfgco.com/isolation-mounts.pdf (damping coefficient for natural rubber)"

[9] Petrillo D., Cavinato A., Gaino M., Chiariotti F., Buonomo M. "FELDs experiment Final Report" *Esa Education*, March 2015

[10] Petrillo D., Cavinato A., Gaino M., Chiariotti F., Buonomo M., et al. "FELDs experiment from design to microgravity testing." *66th IAC, Jerusalem, Israel*, 12 – 16 October 2015

[11] Petrillo D., Cavinato A., Gaino M., Chiariotti F., Buonomo M., et al. "FELDs Experiment: a new flexible soft docking concept" *1st Symposium on Space Educational Activities, Padua, Italy*, 9 – 12 December 2015

[12] Olivieri L., Mantellato R., et al. "Cubesat mission concept for Tethered Electromagnetic Docking demonstration" *Tartu Conference on Space Science and Technology, Tartu, Estonia*

[13] Megson T. "Aircraft Structures for Engineering Students, 5th Edition", 20 February 2012

[14] Serope Kalpakjian, Steven R. Schmid "Tecnologia Meccanica", 2/Ed. italiana, Pearson, 2014

[15] www.feldsexperiment.com

List of Figures

List of Tables

Acronyms

AMDS Autonomous Microsatellite Docking System

ARCADE Autonomous Rendezvous Control And Docking Experiment

CISAS University Center of Studies and Space Activities

CRV Crew Return Vehicle

DLR German Aerospace Center

DYT Drop Your Thesis!

FELDs Flexible Electromagnetic Leash Docking system

FEMM Finite Element Method Magnetics

ISS International Space Station

LEO Low Earth Orbit

NASA National Aeronautics and Space Administration

REXUS/BEXUS Rocket/Baloon Experiment for University Students

SEC Sensor Electromagnet and Cap

SPHERES Synchronized Position Hold, Engage, Reorient, Experimental Satellites

SNBS Swedish National Space Board

ZARM Center of Applied Space Technology and Microgravity

Acknowledgments

I would like to thank Prof. Francesconi for his help and support during the last three years.

Another huge thanks goes to Davide and Marco G., from the beginning we always strive for the best results for FELDs, and to Federico and Marco B. as well, for their valuable work previous, during and after the test campaign.

Finally how i couldn't thanks Francesco B., Francesco S. and Lorenzo for sharing their experience and for guiding us through the complicated first steps.